Regional sources of atmospheric formaldehyde and acetaldehyde, and implications for atmospheric modeling

D.J. Luecken*, W.T. Hutzell, M.Strum, and G.Pouliot

U.S. Environmental Protection Agency, 109 T.W. Alexander Dr., Research Triangle Park, NC, 27709

**corresponding author: Mail Drop E243-03, Tel: +1-919-541-02544, Fax: +1-919-685-3236*
Email address: luecken.deborah@epa.gov

Abstract

Formaldehyde and acetaldehyde concentrations over the Eastern half of the United States are simulated with a 3-D air quality model to identify the most important chemical precursors under January and July conditions. We find that both aldehydes primarily result from photochemical production, although 25% or more result from direct emissions in urban areas during winter. Isoprene is the major precursor of formaldehyde in most areas during summer, contributing 20-60% of total production, with the magnitude being spatially variable. Other alkenes from anthropogenic and/or biogenic emissions dominate formaldehyde production in winter, contributing 60-85% of total formation, and are prominent contributors in summer. Alkenes, including biogenic alkenes, dominate acetaldehyde production during both seasons. These conclusions are based on the degradation of emitted VOCs described by the SAPRC07TB chemical mechanism, but even this detailed model has difficulty reproducing observed values better than a factor of 2. The substantial role of isoprene and other alkenes in aldehyde formation emphasizes that we examine and improve emission estimates of these compounds. Until we can estimate the emissions and understand the chemistry of VOC precursors to aldehyde formation with greater certainty, it will be difficult to accurately predict atmospheric concentrations of aldehydes and develop strategies to reduce their concentrations.

Keywords: Formaldehyde, acetaldehyde, HAPs, photochemical production, isoprene

1.0 Introduction

Formaldehyde (HCHO) and acetaldehyde (CH_3CHO) play important roles in atmospheric photochemistry and air quality. They are a large component of the total VOC reactivity of the atmosphere, providing sources of new radicals that drive ozone formation (Jeffries, 1995; Steiner

et al., 2008; Xie et al., 2011a). They are hazardous air pollutants (HAPs) known or suspected as carcinogens posing health risks (HEI, 2007; Tilgner and Herrmann, 2010; US EPA, 2011). They participate in aqueous chemistry due to their high solubility and interactions with other dissolved species in clouds (Adewuyi et al., 1984; Tilgner and Herrmann, 2010; Warneck, 1989), and contribute to secondary organic aerosols by producing radicals that oxidize hydrocarbons. The chemistry of these two compounds is an indicator of our overall understanding of atmospheric photochemistry. A better understanding of aldehyde production and decay will enable us to develop and analyze policies that consider the effects of air quality measures on a number of different atmospheric pollutants.

Both compounds are emitted directly into the atmosphere from a variety of sources. Anthropogenic emissions of HCHO and CH_3CHO are ubiquitous, concentrated in urban areas, and are among the 25 highest-emitted anthropogenic VOCs in the US (Simon et al., 2010). Mobile sources and stationary combustion dominate anthropogenic sources. Biogenic sources include live and decaying plants, biomass burning, and seawater.

Another source of HCHO and CH_3CHO is secondary formation from degradation of VOCs (Atkinson, 1997; Seinfeld and Pandis, 1998), produced in multiple steps during hydrocarbon oxidation. Equations 1a through 1c show a simple example of HCHO formation from methane (CH_4). Hydrogen abstraction from CH_4, followed by fast addition of oxygen to the alkyl radical (1a) creates a methyl peroxy radical which can oxidize NO to NO_2 (1b), creating a methyl alkoxy radical and eventually leading to ozone formation. A hydrogen atom from the alkoxy radical is abstracted during the reaction with oxygen (1c) along with elimination of HO_2 to form formaldehyde:

$$CH_4 + OH + O_2 \rightarrow CH_3O_2\bullet + H_2O \quad (1a)$$

$$CH_3O_2\bullet + NO \rightarrow CH_3O\bullet + NO_2 \quad (1b)$$

$$CH_3O\bullet + O_2 \rightarrow HCHO + HO_2 \quad (1c)$$

Aldehydes can also be formed from alkoxy radicals after scission of a C-C bond, through photolysis, and through alkoxy radical formation in the absence of nitrogen oxides (NO_x), when reactions of the peroxy radical with HO_2 and other peroxy radicals dominate.

64 Because HCHO and CH_3CHO sources include direct emissions and photochemical
65 production, both sources must be correctly characterized when predicting atmospheric
66 concentrations. The importance of emissions versus photochemistry depends on location, time of
67 day and season, and affects any conclusions about how emission changes might be expected to
68 change aldehydes. An earlier modeling study (Luecken et al., 2006) determined that over 80% of
69 formaldehyde and acetaldehyde was due to secondary production. In urban areas in winter,
70 emissions contributed up to 50%. Statistical techniques have been used with measurements to
71 separate out the two components, concluding that 42% of HCHO is due to primary emissions in
72 Mexico City (Garcia et al., 2006), 44-95% in Los Angeles (Grosjean et al., 1983), and
73 approximately 33%-47% in Houston (Friedfeld et al., 2002; Rappenglück et al., 2010). These
74 measurements represent a "true" value that models must attempt to match, but they are made in
75 cities with large emission sources, and include uncertainties such as unspeciated background
76 contributions. Measurements from a few sites may not represent atmospheric processes at other
77 places and times.

78 Both aldehydes are included in atmospheric chemical mechanisms although their
79 representation varies among mechanisms. A large number of organic compounds participate in
80 atmospheric chemistry and each cannot be explicitly represented in the sequence of secondary,
81 tertiary, quaternary, etc. reactions that result in the production of aldehydes, especially at
82 regional-to-global scales. The Master Chemical Mechanism (MCM) (Saunders et al., 2003)
83 contains over 12,600 reactions for 4500 species, but its size makes it unsuitable for repeated
84 simulations across a large area. Chemical mechanisms in 3-D air quality models (AQMs) are
85 significantly condensed, invoking various assumptions and simplifications in the chemistry.

86 In this study, we use the Community Multiscale Air Quality (CMAQ) model (Byun and
87 Schere, 2006) with the SAPRC07TB chemical mechanism (Hutzell et al., 2011) to track sources
88 of ambient HCHO and CH_3CHO. A recent evaluation of CMAQ with SAPRC07TB has been
89 made for ozone and fine particulate matter ($PM_{2.5}$) components (Hutzell et al., 2011). With this
90 system, we simulate detailed atmospheric photochemical formation and decay of HCHO and
91 CH_3CHO in both low- and high-NOx conditions, within a realistic environment that is affected
92 by atmospheric transport, deposition, precipitation, actinic flux, temperature and pressure
93 gradients, and spatially- and temporally-varying emissions. An increasingly important use of

CMAQ is to assess proposed emission changes on a multipollutant basis, where effects of emission changes on ambient concentrations of ozone, $PM_{2.5}$, and hazardous air pollutants are predicted simultaneously.

The goal of this work is to characterize regional-scale concentrations and chemical sources of atmospheric HCHO and CH_3CHO, and identify which VOCs are the largest producers of these aldehydes. Our analysis differs from previous studies by 1.) explicitly tracking direct emissions and photochemical production, 2.) employing a smaller grid resolution than previous aldehyde modeling studies, 3.) allocating production to specific, emitted compounds, and 4.) examining spatial and temporal differences in contributions. The ability to identify direct and indirect contributions to atmospheric HCHO and CH_3CHO will help us predict how they will respond to emission changes, and guide development of policies that reduce ozone and $PM_{2.5}$ without increasing HAPs. This can also assist in prioritizing research efforts to improve aldehyde predictions, by focusing on those processes likely to have the largest impact on concentrations.

2.0 Methods

The model and methods have been previously described (Hutzell et al., 2011) and are briefly summarized here.

2.1 CMAQ model, domain, boundary conditions and meteorology

We applied CMAQ version 4.7.1 (Foley et al., 2009) with a 36x36 km^2 horizontal grid covering the continental US and a nested 12x12 km^2 grid over the Eastern half of the US (Figure 1). There are 14 vertical layers, extending from the surface up to about 16 km. Boundary conditions for the continental simulations were extracted from the GEOS-CHEM model with those for the nested domain provided by continental CMAQ simulations. Meteorological inputs were obtained from the MM5 meteorological model (http://box.mmm.ucar.edu/mm5/) version 3.6.1. Simulations were performed for two months, January and July, 2002, after a10-day model spin up period.

We created emissions using the 2002 National Emissions Inventory (NEI) (http://www.epa.gov/ttn/chief/net/2002inventory.html). The Sparse Matrix Operator Kernel Emissions (SMOKE) emission processor version 2.4 (http://www.smoke-model.org) was used to

create model ready emissions, with speciation rules (http://www.cert.ucr.edu/~carter/emitdb/) for allocating explicit species to lumped model species. Biogenic emissions were calculated with Biogenic Emissions Inventory System (BEIS) version 3.13. The 2002 HAP inventory was used to estimate HAP emissions and other VOCs were derived from speciation of total VOC emissions (Simon et al., 2010).

2.2 Chemical Mechanism

The SAPRC07 mechanism has been extensively evaluated and described in detail elsewhere (Cai et al., 2010; Carter, 2010). This study uses the SAPRC07TB version, which includes additional explicit high emission and HAP species, including propene, ethanol, 1,2,4-trimethylbenzene, acrolein, 1,3-butadiene, toluene, three isomers of xylene, and α-pinene. The CMAQ implementation of SAPRC07TB (Hutzell et al., 2011) includes temperature and pressure dependencies of the photolysis parameters and extensions for aerosol formation.

2.3 Process and Integrated Reaction Rate Analyses

To quantify contributors to aldehyde formation, we implement the Integrated Reaction Rate (IRR) and Process Analysis (PA) capabilities within CMAQ (Gipson, 1999). This technique has been useful for understanding ozone production and cycling of radicals and nitrogen oxides (Jang et al., 1995; Jeffries and Tonnesen, 1994). We use IRR to track radical and oxidized intermediates which form HCHO and CH_3CHO, such as peroxy and acyl peroxy radicals, methyl vinyl ketone and methyl ethyl ketone and allocate these intermediates to stable species which are emitted. Products from all VOC reactions are tracked if they eventually react to form either HCHO or CH_3CHO. The entire chemical mechanism is utilized for the CMAQ simulation (Hutzell et al., 2011), and we use IRR within the simulation to quantify the HCHO and/or CH_3CHO produced through 251 organic reactions (Supplementary Information, Table S-1). This information is post-processed to quantify HCHO and/or CH_3CHO produced from emitted organic species.

Since some VOCs are both emitted and produced photochemically, we separate the emitted portion from that formed photochemically, which we track to its precursors. For example, the model species representing methyl ethyl ketone and similar ketones (MEK), an

156 emitted VOC, produces HCHO via acetyl and methyl peroxy radicals. But MEK can itself be
157 produced by isoprene as a second generation product. We calculate the fraction of MEK
158 concentration at each hour due to emissions, which ranges from 10-95%, depending on location,
159 and use that to apportion HCHO to either MEK emissions or its precursors (in this example,
160 isoprene). Similarly, we separate the formation of HCHO from CH_3CHO into that fraction due
161 to emissions and to chemistry. We assume that model species transported into the grid cell have
162 the same ratio of formation versus emission as the current grid cell. We list results for four
163 explicit species (isoprene, methane, acetaldehyde and ethanol) and 9 lumped chemical
164 categories:

165 • alkanes: non-methane alkanes lumped in model species ALK1 through ALK5
166 • ethene and propene
167 • lumped alkenes: model species OLE1 and OLE2
168 • aromatics: benzene, m-,p- and o-xylene, toluene, 1,2,4-trimethylbenzene, and
169 model species ARO1 and ARO2
170 • terpenes and pinenes: α-pinene and model species SESQ and TERP, representing
171 sesquiterpenes and other terpenes
172 • PANs: peroxyacetyl nitrate, peroxymethacryloyl nitrate, and model species PAN2
173 (peroxypriopionyl nitrate and higher PANs) and PBZN (from aromatic aldehydes)
174 • C3+ aldehydes: model species RCHO representing aldehydes with 3 or more
175 carbons
176 • lumped oxygenates: methylglyoxal, acetone, and model species MEK, lumped
177 ketones (PRD2 and IPRD) and isoprene products (IPRD)
178 • other: species that individually produce <1% of total formation.
179
180 We selected 10 locations throughout the domain, shown in Figure 1, for performing IRR
181 analyses, to examine how different chemical regimes and emissions mixes affect aldehyde
182 precursors. These locations include five grid cells examined previously (Hutzell et al., 2011) for
183 their oxidant chemistry (Louisville, Baltimore, Atlanta, Alabama, N. Georgia), three rural
184 locations (Alabama, E. Pennsylvania, N. Georgia), and five urban locations where measurements
185 are available in 2002 for comparison (Chicago, Baltimore, New York, Houston, Minneapolis).

These locations, defined by processes within a 12x12 km^2 grid cell at the given location, are not meant to fully characterize specific cities or regions, but do display the range of variability expected in contributors to aldehyde formation.

3. Results and Discussion

3.1 Regional concentrations and impact of direct emissions versus photochemical production

We focus on results over the Eastern nested domain because the finer scale more accurately characterizes spatial variability in meteorological and photochemical processes. Figure 2 shows monthly-averaged concentrations of HCHO in January and July, and fraction of overall concentration due to photochemistry. The remainder is attributed to direct HCHO emissions.

In Figure 2, modeled HCHO concentrations are higher in July than January, by over a factor of 4, due to higher actinic flux, radical concentrations and precursor emissions of biogenic VOCs in summer. During winter, concentrations are highest in urban areas where emissions of HCHO are largest; in these areas emissions account for 25-50% of total HCHO. During summer, HCHO emissions contribute much less: 6-25% . The photochemical contribution and concentration of HCHO is highest in the Southeast, consistent with satellite observations (Millet et al., 2008; Palmer et al., 2006) and earlier modeling results (Luecken et al., 2006).

Figure 3 shows concentrations and emission fractions for CH_3CHO. The seasonal patterns are similar to HCHO, but concentrations are lower by half and the contribution of photochemistry is greater, accounting for over 80% of total CH_3CHO in winter and 95% in summer.

Figure 4 displays seasonal differences in the role of emissions versus production at the 10 locations, and the average over the entire domain. For this sampling of grid cells, primary emissions contribute at most 55% of the HCHO in January (Louisville). In summer, emissions contribute less than 20% at all locations.

3.2 Chemical precursors of aldehydes

Relative contributions of different VOCs to aldehyde production depend on the magnitude of emissions and yield of aldehydes per molecule of reacting VOC. We use IRR and PA analyses to quantify the role of different VOCs by summing reaction rates and yields over two periods: January 14-16, 2002 and July 15-17, 2002, focusing on 10 locations.

Fractional HCHO formation attributed to individual VOCs and lumped classes is shown in Figure 5. In general, isoprene is the dominant precursor of HCHO during July, although the contribution varies spatially. In the Southeast, such as the location near urban Atlanta, isoprene contributes approximately 50-65% of total formation. In the Mid Atlantic location near Baltimore, isoprene contributes approximately 20% of HCHO formation. The reaction of isoprene with OH dominates HCHO formation when isoprene is present, accounting for 75-95% of HCHO attributed to isoprene, largely through an operator (xHCHO) which yields 80-99% HCHO in later sequences. Another operator produced by isoprene (xIPRD), produces reactive oxygenated products (IPRD), providing an additional 3-8% HCHO formation. During January, when emissions of isoprene are reduced, production is dominated by lumped and explicit alkenes. In the locations near New York and Louisville, explicit and lumped alkenes are larger contributors than isoprene, even in July. Methane and other alkanes also contribute to HCHO formation.

Figure 6 displays VOC contributors to CH_3CHO production. Isoprene plays a minor role in CH_3CHO production, and alkenes contribute the largest amount. Terpenes and cyclic terpenes are major contributors in Southeastern locations. Alkanes and PANs, particularly peroxyproprional nitrate, contribute in some locations. Ethanol contributes up to 5% of CH_3CHO production, and indirectly produces HCHO through CH_3CHO decay.

While lumped alkenes are the largest relative contributors in January, the absolute contribution of these compounds to HCHO and CH_3CHO formation is smaller than in July. Both compounds are formed in larger amounts in summer (20-50 times higher for HCHO and 7-40 times higher for CH_3CHO) because the major reaction involves the hydroxyl radical (OH), which can be 5 times or more higher in summer than winter (Ren et al., 2006). Supplementary Figure S-1 shows a comparison of the total production of HCHO and CH_3CHO from lumped alkenes for both periods. Additional factors, such as warmer temperatures, higher actinic fluxes and greater

biogenic emissions increase formation in summer. The same seasonal factors that cause higher production rates via OH also cause higher destruction through OH, so concentration differences between summer and winter are not as large as suggested by formation rate differences (Figures 2 and 3).

3.3 Comparisons of model results with observations

Figure 7 compares modeled HCHO and CH_3CHO with 1, 3 and 24 hr-averaged observations from the PAMs network (www.epa.gov/air/oaqps/pams), where the sites are differentiated by state. The observations are limited and insufficient for fully evaluating the model, but do serve as a touchstone to determine whether model predictions are realistic. One limitation of these observations is that sampling frequency varies: some sites report every day, others report every 3-12 days or longer, sometimes only one measurement is reported during the month. In addition, the monitoring sites are sparse and unevenly distributed spatially, making it difficult to evaluate predictions from a regional model. In July, 1299 observations from 96 sites were available, versus over 41 million model surface predictions, so we are evaluating only a small fraction of predicted values. In January, only 79 sites and 331 observations were available. Observations are particularly lacking in rural areas and the Southeast where high isoprene emissions and HCHO concentrations are predicted.

In comparison with these limited observations, both compounds are underestimated by the CMAQ simulations, especially at higher concentrations. In July, the mean bias (MB) is -4 ppb, and normalized mean bias (NMB) is -0.59. When the highest 5% of observed values are removed, some of which are extremely high, the MB is reduced to -2.43 and NMB to -0.47. In January, the MB is -1.5 and NMB is -0.69, while with the top 5% of values removed, the MB is -0.83 and NMB is -0.55. In many states the bias is much less. It is unclear why some states are modeled well but others underpredicted. At some sites, such as those located around Chicago (IL), and Minneapolis (MN), the model matches predictions well, while others, including New York (NY) and RI are modeled 50% too low. Others, including the Baltimore site (MD) fall in between.

Previous attempts to model HCHO had limited success; sometimes models overpredict, but more often underpredict measured values at the surface. Previous comparisons of CMAQ

275 predictions for HAPs (Luecken et al., 2006) showed that observations could generally be
276 predicted within a factor or two. Comparisons of a box model and GEOS-CHEM predictions
277 against data from the 2004 INTEX campaign (Fried et al., 2008) similarly showed 50%
278 underpredictions.

279 Several possible causes of differences between models and measurements have been
280 noted previously. One cause is error in the measurements. Numerous studies have identified
281 interferences in measurements of HCHO and CH_3CHO (Arnts and Tejada, 1989; Herrington et
282 al., 2006; Karst et al., 1993; Sirju and Shepson, 1995), which can cause positive or negative
283 biases. Another possible cause is mismatch between point measurements and volume average
284 concentrations predicted by models. The presence of large, localized sources may explain the
285 inability of a 12 x 12 km^2 grid cell to capture the highest values. In a few cases, these values are
286 abnormally high: one site in Michigan reports a 24-hour average HCHO concentration on July
287 13, 2002 of 71.1 $\mu g\ m^{-3}$, while the next measurement on July 25 is 4.81 $\mu g\ m^{-3}$. This monitor is
288 south of downtown Detroit, in an area with industrial units, residential housing and highway
289 traffic, so it could be influenced by intermittent high point emissions. A nearby monitor reported
290 5.79 $\mu g\ m^{-3}$ on July 13.

291 Other errors could occur in specification of emissions or chemistry. To identify the
292 largest potential sources of error causing underpredictions, we use information from Section 3 to
293 focus on those chemicals with the largest influence on aldehyde predictions. We discuss the
294 potential magnitude of uncertainties in emissions and chemistry of these VOCs, to prioritize
295 areas for improving aldehyde predictions.
296
297 **4.0 Implications for modeling the atmospheric chemistry of aldehydes**
298
299 Our ability to accurately predict ambient concentrations of formaldehyde and
300 acetaldehyde depends on our ability to predict concentrations of all VOCs. In this section, we
301 examine factors influencing the concentrations of the most important VOC precursors identified
302 in Section 3.2. We first discuss uncertainties involved in modeling emissions, and then
303 uncertainty in modeling the chemistry of these compounds.

304 4.1 Aldehyde emissions and decay

Emissions of HCHO and CH_3CHO can be important sources of ambient concentrations, but atmospheric production is generally larger (Figures 2 and 3). For both aldehydes, emissions derived from the NEI are less than emissions derived from total VOC emissions applying speciation profiles (Simon et al., 2010). Differences between the two values may be caused by lack of reporting requirements, different emission factors and speciation profiles. In the most extreme case (Louisville in January), using speciation profiles instead of the NEI could increase our modeled HCHO concentrations by a maximum of 50% and CH_3CHO by 30% in winter, and HCHO up to 20% in summer, reducing some underprediction. In other areas, especially in summer, the change would only be a few percent. This suggests that direct emissions of formaldehyde and acetaldehyde are not likely to be the only cause of model underprediction. Emissions of larger aldehydes and subsequent photochemical decay are also a source of smaller aldehydes, and errors in these emissions could also increase the HCHO up to 24% and CH_3CHO up to 29%.

The photochemical loss reactions of HCHO and CH_3CHO have been well studied and are not likely to have major errors. Slightly more than half of the photochemical loss is through photolysis, with most of the remainder from reaction with OH.

4.2 Isoprene

Isoprene has been identified as a major contributor to HCHO in summer (Carslaw et al., 2000; Millet et al., 2006; Sumner et al., 2001), consistent with our study. Our results also show a substantial degree of spatial variability across the region, with contributions less than 20% in some areas. In rural locations, isoprene contributes about half of the HCHO production in summer. The ability to accurately predict HCHO concentrations in summer strongly depends on accurately predicting isoprene concentrations, which depends on accurately representing both isoprene emissions and chemistry.

Isoprene is almost entirely emitted by biogenic sources and estimates of the source strength are uncertain over regional scales. Several models of isoprene emissions are available, but they give different estimates. A comparison of four models showed a factor of two differences among models (Warneke et al., 2010). In modeling studies using BEIS, isoprene concentrations are

underestimated (Doraiswamy et al., 2009), overestimated (Wiedinmyer et al., 2005) and reasonably well estimated (Hogrefe et al., 2011). Table 2 shows examples of differences that might be seen between inventories developed using two different models for biogenic emissions; the BEIS and MEGAN (Guenther et al., 2006) models, at each of the 10 locations. Isoprene emissions estimated by these two models can differ by 75% or more, with emissions from MEGAN generally larger than BEIS. A factor of 2 error in isoprene emissions could increase modeled formaldehyde by up to 80%. The large influence of isoprene on HCHO combined with large uncertainties in the emissions of isoprene introduces significant uncertainties in HCHO predictions.

The atmospheric chemistry of isoprene is currently being re-examined, and it is unclear how updated isoprene chemistry will affect predictions of HCHO. Inclusion of the 1,5-H isomerization reactions of β-hydroxyalkenyl peroxy radicals increased OH, and this channel would increase the HCHO production proportionally (Archibald et al., 2010a). Similarly, consideration of the 1,6-H shift leads to hydroperoxy aldehydes, yielding additional HCHO after rapid photolysis, along with OH and HO_2 (Peeters, 2010; Stavrakou et al., 2010). Increased OH radical regeneration in nonurban environments could increase production of HCHO through other VOCs. Updated isoprene chemical reactions can have significantly higher HCHO yields from δ-hydroxy isoprene nitrates (Paulot et al., 2009), and using this chemistry in CMAQ can potentially increase modeled HCHO less than 10% overall (Xie et al., 2011b). A critical evaluation of reaction products must be performed for any new isoprene mechanism. Because no consensus has yet been reached on the best way to represent isoprene chemistry, we offer no recommendation here on improvements, but do expect it will affect HCHO.

4.3 α-pinene, terpenes and sesquiterpenes

The terpenes and cyclic terpenes are known contributors to SOA formation, and this analysis shows that they also contribute to aldehyde formation. Acetaldehyde (up to 25%) and formaldehyde (6%) production depends on correctly estimating emissions of terpenes. These results agree with a previous analysis over Europe (Dufour et al., 2009) in which terpene emissions accounted for 8% of average CH_3CHO in Western Europe, and up to 25% locally. Like isoprene, these chemicals are almost entirely biogenic but their emissions have not been

studied in as much detail. We conclude that a similar uncertainty as isoprene is likely; uncertainty of a factor of 2 could increase acetaldehyde concentrations by 25%.

The chemistry of terpenes beyond first generation products is also not well known, and many assumptions were made in its condensed representation. A comparison of SAPRC07 with the MCM, which has a more complete description of intermediate chemistry, found that MCM predicted 2.3 times the photochemical ozone creation potential (POCP) for α-pinene than SAPRC07, almost twice as much for β-pinene, and 2.8 times more than limonene. This was attributed to different treatments of degradation chemistry beyond first generation products (Derwent et al., 2010). While ozone reactivity is not the same as aldehyde formation, they both occur through similar pathways and it is possible that aldehyde formation would be similarly lower in SAPRC07TB. If the mechanistic reactivity of the terpenes is underrepresented in SAPRC07TB by a factor of 2, the CH_3CHO might be expected to increase up to 25%.

4.4 Other alkenes

Other alkenes, including ethene, propene, and larger alkenes and dienes, are major contributors to both HCHO and CH_3CHO formation, especially in the January simulation. In a previous allocation of acetaldehyde sources (Millet et al., 2010), alkenes were about half as important as alkanes and slightly larger than ethanol. This contrasts with our findings, where alkenes contribute the majority of acetaldehyde production, perhaps due to inclusion of biogenic emissions. Many biogenic alkenes that are not isoprene or terpenes, such as 2-methyl-3-butene-2-ol, are lumped in OLE1 and OLE2. Table 2 lists the fraction of lumped alkenes from biogenic sources at each of the 10 locations (Supplementary Figure S-2 shows the fraction across the Eastern US). In contrast to isoprene, alkenes from MEGAN are generally lower than BEIS for most locations, so using MEGAN would lower aldehyde production through alkenes. Are there reactive VOCs not predicted by MEGAN or BEIS that might contribute to HCHO formation? Photochemical modeling at Blodgett Forest (Choi et al., 2010) could not reconcile measured and modeled HCHO concentrations, postulating a missing reactive biogenic VOC source. Other analyses (Kim et al., 2011) found no evidence for significant missing biogenic VOCs in a branch enclosure measuring OH reactivity, and attribute discrepancies to unmeasured isoprene oxidation

394 products. It is unclear whether errors in biogenic alkene emissions are a major source of
395 aldehyde model underpredictions.

396 Anthropogenic sources of lumped alkenes have equal or greater importance for aldehyde
397 formation at all locations in winter, and urban locations in summer. Studies in Houston, Texas
398 (Wert et al., 2003) agree with our study by pointing to anthropogenic emissions of propene and
399 ethene as major HCHO precursors. Figure 8 shows fifteen alkenes with the highest emissions
400 and general source categories from which they are emitted (Simon et al., 2010). Mobile sources
401 are the largest source of alkenes, along with emissions from general industrial sources, stationary
402 combustion, and waste disposal, treatment and recovery. Mobile source estimation methods rely
403 on models that account for emission differences due to fuel type, vehicle technology, speed,
404 temperature, and modes of operation. There are uncertainties in the variability of vehicle fleets
405 and fuels across the country, and in parameters used to convert monthly modeled emissions to
406 hourly gridded emissions needed by models. For mobile sources, VOC speciation is generally
407 well-characterized, and comparisons for HAP species such as HCHO and CH_3CHO, which are
408 reported both in the NEI inventory and computed from VOC speciation, are generally within
409 25% (Simon et al., 2010). Comparisons between emissions from the current MOBILE6
410 emissions model and the newer MOVES model show that mobile source VOC emissions from
411 MOVES are similar to those from MOBILE6, sometimes slightly lower (Cook et al., 2010;
412 Houyoux et al., 2009), or slightly higher (Kite, 2011).

413 It is difficult to evaluate integrated emission inventories using ambient observations
414 because measured concentrations include effects of meteorology, deposition, chemistry and
415 emissions. In a comparison of measurements in the Pacific Northwest with CMAQ modeling,
416 the VOC reactivity of propene was overpredicted; reduction of the VOC inventory by 30% was
417 needed for the model to match afternoon observations of ozone production efficiency (Xie et al.,
418 2011a). Similarly, a modeling study using CMAQ in the Northeastern US found that modeled
419 ethene concentrations generally overpredicted morning measurements by 20-100% (Doraiswamy
420 et al., 2009). In contrast, an analysis using emission ratios found that inventories of alkenes in
421 the NEI were underpredicted (Warneke et al., 2007). It is unclear whether anthropogenic alkene
422 emissions in the NEI are too high or low; while errors in the inventory might increase HCHO
423 and CH_3CHO by 22 and 24% in the winter, they might also decrease predictions.

Beyond the simplest alkenes, chemistry becomes more complex, and reactions cannot be easily generalized in a condensed mechanism. Numerous unsaturated compounds are emitted but SAPRC07TB only represents ethene and propene explicitly; the rest are grouped into two model species, OLE1 and OLE2, depending on reaction with OH. On a regional basis, ethene, propene and methyl-substituted butenes make up a majority of alkene emissions (Figure 8). Reactions of these alkenes with OH - the most important decay pathway - have estimated uncertainties of 20-30% (Calvert et al., 2000). In these reactions, the description of β-hydroxy peroxy and alkoxy radical reactions that follow the initial reactions have either been measured or estimated, and explicitly representing glycoaldehyde in SAPRC07TB allows for accurate representation of the fate of β-hydroxyalkoxy radicals from ethene. For larger alkenes, isomerization and reaction with oxygen play a larger role. Reactions of alkenes with ozone are less straightforward - reactions of Criegee intermediates and OH radical generation is an area requiring additional laboratory and modeling studies (Calvert et al., 2000). A 30% uncertainty in chemistry could change aldehyde predictions by 3-24%, although concentrations could increase or decrease.

4.5 Alkanes

Methane and other alkanes contribute to HCHO and CH_3CHO formation. Simulations using the CHIMERE model (Dufour et al., 2009) also identified methane as the dominant source of HCHO in Western Europe, with isoprene playing a lesser role. Despite the low reactivity of methane (maximum incremental reactivity for ozone 0.001 times that of isoprene) and exclusion from the definition of VOC in the United States (US GPO, 2011), large emissions make methane an important hemispheric driver of atmospheric photochemistry. Methane contributes to ozone formation (Fiore et al., 2008; Jeffries, 1995); our results finds methane is also an important contributor to HCHO. Larger alkanes can contribute up to 20% of CH_3CHO formation.

Anthropogenic sources of alkanes generally dominate biogenic sources in our simulations. Figure 9 shows annual emissions of methane and the fifteen largest VOC alkanes. Mobile sources are important, along with other industrial, waste and transport emissions. Landfills are a major source of methane, while storage and transport of petroleum contributes to n-butane emissions. Anthropogenic emissions from the NEI have been reported to differ from emission ratios in the Northeastern US by up to an order of magnitude (Warneke et al., 2007)

454 based on measurements and calculated photochemical age. These discrepancies with the NEI
455 must be further examined to quantify uncertainty in alkane emissions.

456 Alkane chemistry is generally better understood than other species, although the
457 representation of larger and multifunctional alkanes in air quality models is highly condensed.
458 Despite uncertainties inherent in representing a large number of species by a small subset,
459 Derwent et al. (2010) found that the POCP of alkanes modeled with SAPRC07 correlated well
460 with those using MCM, a more detailed representation. This gives confidence that SAPRC07 is
461 representing our knowledge of alkane degradation similarly to MCM.

462 4.6 Ethanol

463 Potential changes in acetaldehyde concentrations from fuel reformulation has been
464 recently studied (Cook et al., 2011; Jacobson, 2007). Our simulations predict ethanol contributes
465 only 3-6% of photochemically-produced acetaldehyde. One recent study (Millet et al., 2010)
466 calculated that converting the US vehicle fleet to 85% ethanol fuel would increase acetaldehyde
467 emissions by 21% and double ethanol emissions. We estimate that such a change would increase
468 acetaldehyde by an average of 6%, possibly more near roadways. Using ethanol fuels will affect
469 concentrations of other VOCs (Cook et al., 2011; Graham et al., 2008; Jacobson, 2007; US EPA,
470 2010), which could be as important as changes in CH_3CHO or ethanol. Changes in alkene
471 emissions, in particular, would impact acetaldehyde. Effects of fuel reformulations on these
472 other VOCs must be accurately characterized to predict their impact on acetaldehyde.

473 4.7 Other chemicals

474 Our analysis does not find a major role for aromatic compounds in producing HCHO or
475 CH_3CHO. While aromatic chemistry is still uncertain, even a major increase in HCHO formation
476 from aromatics would not make them significant compared to other chemicals.

477 Emissions of methanol and acetone (part of the lumped oxygenates category) contribute
478 less than 2% of total HCHO. Recent analyses of aircraft data in the Pacific Northwest (Xie et al.,
479 2011a) postulate that emissions of methanol and acetone would have to increase by factors of 30
480 and 25, respectively, to account for observed values of these compounds. If acetone emissions
481 were 25 times too low in the domain modeled here, HCHO could increase by nearly 20%,
482 bringing the modeled values closer to observations. Increasing methanol would increase its role

483 in HCHO formation similarly, but isoprene would continue to remain the most important
484 precursor in most areas in summer. Neither methanol nor acetone is considered a VOC (US
485 GPO, 2011) and must be derived from inventories of total organic gas.

486 Lastly, is it possible that our simulations underestimate OH radical concentrations, thus
487 underestimating a critical first step in degradation of stable VOCs? Studies comparing box
488 model predictions to measurements find both underestimates (Chen et al., 2010; Hofzumahaus et
489 al., 2009) and some overestimates (Emmerson et al., 2007). Measurements of OH and HO_2 are
490 difficult so mechanisms have not been thoroughly evaluated for predictions of these radicals.
491 OH participates in both HCHO production and decay, so errors in OH will not change HCHO in
492 a linear fashion. If OH is larger than predicted by SAPRC07TB, this would explain some of the
493 HCHO and CH_3CHO underpredictions.

494

495 **5.0 Summary**

496 Because the chemistry of HCHO and CH_3CHO is integral to almost all VOC decay and
497 production pathways, it reflects our current understanding of VOC photochemistry and tests our
498 entire mechanistic understanding of atmospheric chemistry. To accurately model their
499 concentrations, we must correctly account for emissions, transport, deposition, and the
500 degradation chemistry of not only aldehydes, but also VOC precursors to aldehydes. In this
501 study we conclude that:

502 1. Atmospheric photochemical production accounts for most of the HCHO and
503 CH_3CHO concentrations in the ambient atmosphere. Aside from dense
504 urban/industrial areas, reduction of HCHO and CH_3CHO emissions is expected to
505 have a small effect on reducing concentrations. In a few areas, especially in winter,
506 emissions are important and a large source of uncertainty is differences between
507 emissions from the NEI and emissions based on speciated VOC.
508 2. Substantial spatial and seasonal variation occurs in how much various VOCs
509 contribute to photochemical production of aldehydes. For example, isoprene is not
510 always the dominant VOC producing HCHO, even during summer.

3. Biogenic emissions of compounds that photochemically react to produce HCHO and CH_3CHO are highly uncertain and a potential source of error in aldehyde predictions.
4. Resolving uncertainties in the chemistry of isoprene and other alkenes is critical for chemical mechanisms to accurately predict concentrations of aldehydes. Newly proposed isoprene mechanisms must be evaluated for a wide range of species, including HCHO.
5. Anthropogenic alkenes, largely from mobile sources, play an important role in aldehyde formation. While mobile sources are perhaps better represented in the NEI than other categories, new uncertainties are constantly being introduced by changes in vehicles and fuels.
6. The CMAQ air quality model tends to underpredict aldehyde concentrations. At many sites this underprediction is close to 50%.

While much effort has spent developing condensed chemical mechanisms that are as representative of the underlying chemicals as possible, there will necessarily be compromises. Even the most explicit mechanisms, such as the MCM, rely on some degree of condensation. It is encouraging that comparisons between explicit mechanisms and condensed mechanisms are generally consistent (Archibald et al., 2010b; Derwent et al., 2010), although carbonyls tend to be one class of compounds which are often predicted differently among mechanisms.

The general underprediction of air quality models for aldehydes is an area which requires more investigation. Because aldehyde decay is a large source of new radicals which drive photochemistry, this raises questions about the robustness of predictions for other photochemical pollutants, such as ozone and $PM_{2.5}$; species which air quality models predict well. HCHO, in particular, is an important ozone precursor.

Our findings on the most significant chemical sources of HCHO and CH_3CHO are based on our best assessment of emissions and chemistry on a regional scale. The existence of many uncertainties implies that the contributions of different VOCs to aldehyde formation may change somewhat as our knowledge of chemistry and emissions improves. Refining our understanding of aldehyde behavior in the atmosphere is an iterative and imperfect process involving measurements, modeling, and collecting improved data on emission sources. New information

will help to more accurately bound our understanding of how air quality might change under future emissions scenarios, and build confidence in using regional models for air quality management and research.

6.0 Acknowledgments

The authors acknowledge helpful discussions with our US EPA colleagues Ted Palma and Ying Xie, and with William Carter, who developed this SAPRC07TB mechanism. We greatly appreciate the numerous helpful suggestions from our internal and external reviewers, all of whom have helped focused the purpose of this manuscript and clarified the presentation. The United States Environmental Protection Agency, through its Office of Research and Development, funded and managed the research described here. It has been subjected to Agency administrative review and approved for publication.

7.0 References

Adewuyi, Y.G., Cho, S.-Y., Tsay, R.-P., Carmichael, G.R., 1984. Importance of formaldehyde in cloud chemistry. Atmospheric Environment 18, 2413-2420.

Archibald, A.T., Cooke, M.C., Utembe, S.R., Shallcross, D.E., Derwent, R.G., Jenkin, M.E., 2010a. Impacts of mechanistic changes on HOx formation and recycling in the oxidation of isoprene. Atmospheric Chemistry Physics 10, 8097-8118.

Archibald, A.T., Jenkin, M.E., Shallcross, D.E., 2010b. An isoprene mechanism intercomparison. Atmospheric Environment 44, 5356-5364.

Arnts, R.R., Tejada, S.B., 1989. 2,4-Dinitrophenylhydrazine-coated silica gel cartridge method for determination of formaldehyde in air: identification of an ozone interference. Environmental Science & Technology 23, 1428-1430.

Atkinson, R., 1997. Gas-phase tropospheric chemistry of volatile organic compounds: 1. alkanes and alkenes. Journal of Physical and Chemical Reference Data 26, 215-290.

Byun, D., Schere, K.L., 2006. Review of the Governing Equations, Computational Algorithms, and Other Components of the Models-3 Community Multiscale Air Quality (CMAQ) Modeling System. Applied Mechanics Reviews 59, 51-77.

Cai, C., Kelly, J.T., Avise, J.C., Kaduwela, A.P., Stockwell, W.R., 2010. Implementation of the SAPRC07C chemical mechanism in the Community Multiscale Air Quality (CMAQ) model for photochemical modeling in California: Comparisons with SAPRC99. Journal of the Air & Waste Management Association submitted.

Calvert, J.G., Atkinson, R., Kerr, J.A., Madronich, S., Moortgat, G.K., Wallington, T.J., Yarwood, G., 2000. The mechanisms of atmospheric oxidation of the alkenes. Oxford University Press, New York/Oxford.

574 Carslaw, N., Bell, N., Lewis, A.C., McQuaid, J.B., Pilling, M.J., 2000. A detailed case study of
575 isoprene chemistry during the EASE96 Mace Head campaign. Atmospheric Environment 34,
576 2827-2836.

577 Carter, W.P.L., 2010. Development of the SAPRC-07 chemical mechanism. Atmospheric
578 Environment 44, 5324-5335.

579 Chen, S., Ren, X., Mao, J., Chen, Z., Brune, W.H., Lefer, B., Rappenglück, B., Flynn, J., Olson,
580 J., Crawford, J.H., 2010. A comparison of chemical mechanisms based on TRAMP-2006 field
581 data. Atmospheric Environment 44, 4116-4125.

582 Choi, W., Faloona, I.C., Bouvier-Brown, N.C., McKay, M., Goldstein, A.H., Mao, J., Brune,
583 W.H., LaFranchi, B.W., Cohen, R.C., Wolfe, G.M., Thornton, J.A., Sonnenfroh, D.M., Millet,
584 D.B., 2010. Observations of elevated formaldehyde over a forest canopy suggest missing sources
585 from rapid oxidation of arboreal hydrocarbons. Atmospheric Chemistry Physics 10, 8761-8781.

586 Cook, R., Glover, E., Yanca, C., Warila, J., Sales, A., 2010. Modeling air toxics in EPA's
587 MOVES emissions model, 2010 Coordinating Research Council Air Toxics Workshop.
588 Coordinating Research Council, Sacramento, CA.

589 Cook, R., Phillips, S., Houyoux, M., Dolwick, P., Mason, R., Yanca, C., Zawacki, M., Davidson,
590 K., Michaels, H., Harvey, C., Somers, J., Luecken, D., 2011. Air quality impacts of increased use
591 of ethanol under the United States' Energy Independence and Security Act. Atmospheric
592 Environment, in Press.

593 Derwent, R.G., Jenkin, M.E., Pilling, M.J., Carter, W.P.L., Kaduwela, A., 2010. Reactivity
594 Scales as Comparative Tools for Chemical Mechanisms Journal of the Air & Waste
595 Management Association 60, 914-924.

596 Doraiswamy, P., Hogrefe, C., Hao, W., Henry, R.F., Civerolo, K., Ku, J.-Y., Sistla, G., Schwab,
597 J.J., Demerjian, K.L., 2009. A diagnostic comparison of measured and model-predicted speciated
598 VOC concentrations. Atmospheric Environment 43, 5759-5770.

599 Dufour, G., Wittrock, F., Camredon, M., Beekmann, M., Richter, A., Aumont, B., Burrows, J.P.,
600 2009. SCIAMACHY formaldehyde observations: constraint for isoprene emission estimates over
601 Europe? Atmospheric Chemistry Physics 9, 1647-1664.

602 Emmerson, K.M., Carslaw, N., Carslaw, D.C., Lee, J.D., McFiggans, G., Bloss, W.J.,
603 Gravestock, T., Heard, D.E., Hopkins, J., Ingham, T., Pilling, M.J., Smith, S.C., Jacob, M.,
604 Monks, P.S., 2007. Free radical modelling studies during the UK TORCH Campaign in Summer
605 2003. Atmospheric Chemistry Physics 7, 167-181.

606 Fiore, A.M., West, J.J., Horowitz, L.W., Naik, V., Schwarzkopf, M.D., 2008. Characterizing the
607 tropospheric ozone response to methane emission controls and the benefits to climate and air
608 quality. Journal of Geophysical Research 113, D08307.

609 Foley, K.M., Roselle, S.J., Appel, K.W., Bhave, P.V., Pleim, J.E., Otte, T.L., Mathur, R., Sarwar,
610 G., Young, J.O., Gilliam, R.C., Nolte, C.G., Kelly, J.T., Gilliland, A.B., Bash, J.O., 2009.

611 Incremental testing of the community multiscale air quality (CMAQ) modeling system version
612 4.7. Geoscientific Model Development Discussions 2, 1245-1297.

613 Fried, A., Walega, J.G., Olson, J.R., Crawford, J.H., Chen, G., Weibring, P., Richter, D., Roller,
614 C., Tittel, F.K., Heikes, B.G., Snow, J.A., Shen, H., O'Sullivan, D.W., Porter, M., Fuelberg, H.,
615 Halland, J., Millet, D.B., 2008. Formaldehyde over North America and the North Atlantic during
616 the summer 2004 INTEX campaign: Methods, observed distributions, and measurement-model
617 comparisons. Journal of Geophysical Research 113, D10302.

618 Friedfeld, S., Fraser, M., Ensor, K., Tribble, S., Rehle, D., Leleux, D., Tittel, F., 2002. Statistical
619 analysis of primary and secondary atmospheric formaldehyde. Atmospheric Environment 36,
620 4767-4775.

621 Garcia, A.R., Volkamer, R., Molina, L.T., Molina, M.J., Samuelson, J., Mellqvist, J., Galle, B.,
622 Herndon, S.C., Kolb, C.E., 2006. Separation of emitted and photochemical formaldehyde in
623 Mexico City using a statistical analysis and a new pair of gas-phase tracers. Atmos. Chem. Phys.
624 6, 4545-4557.

625 Gipson, G.L., 1999. Process Analysis, in: D.W., B., Ching, J.K.S. (Eds.), Science Algorithms of
626 the EPA Models-3 Community Multiscale Air Quality (CMAQ) Modeling System. U.S. EPA,
627 Washington, DC, pp. 16-11 to 16-39.

628 Graham, L.A., Belisle, S.L., Baas, C.-L., 2008. Emissions from light duty gasoline vehicles
629 operating on low blend ethanol gasoline and E85. Atmospheric Environment 42, 4498-4516.

630 Grosjean, D., Swanson, R.D., Ellis, C., 1983. Carbonyls in Los Angeles air: Contribution of
631 direct emissions and photochemistry. The Science of The Total Environment 29, 65-85.

632 Guenther, A., Karl, T., Harley, P., Wiedinmyer, C., Palmer, P.I., Geron, C., 2006. Estimates of
633 global terrestrial isoprene emissions using MEGAN (Model of Emissions of Gases and Aerosols
634 from Nature). Atmospheric Chemistry Physics 6, 3181-3210.

635 HEI, 2007. Mobile-Source Air Toxics: A Critical Review of the Literature on Exposure and
636 Health Effects, in: Panel, H.A.T.R. (Ed.). Health Effects Institute, Boston, Massachusetts.

637 Herrington, J.S., Fan, Z.-H., Lioy, P.J., Zhang, J., 2006. Low Acetaldehyde Collection
638 Efficiencies for 24-Hour Sampling with 2,4-Dinitrophenylhydrazine (DNPH)-Coated Solid
639 Sorbents. Environmental Science & Technology 41, 580-585.

640 Hofzumahaus, A., Rohrer, F., Lu, K., Bohn, B., Brauers, T., Chang, C.-C., Fuchs, H., Holland,
641 F., Kita, K., Kondo, Y., Li, X., Lou, S., Shao, M., Zeng, L., Wahner, A., Zhang, Y., 2009.
642 Amplified Trace Gas Removal in the Troposphere. Science 324, 1702-1704.

643 Hogrefe, C., Isukapalli, S.S., Tang, X., Georgopoulos, P., He, S., Zalewsky, E.E., Hao, W., Ku,
644 J.-Y., Key, T., Sistla, G., 2011. Impact of biogenic emission uncertainties on the simulated
645 response of ozone and fine particulate matter to anthropogenic emission reductions. Journal of
646 the Air & Waste Management Association 61, 92-108.

647 Houyoux, M., Strum, M., Mason, R., Dolwick, P., Michaels, H., Huang, A., Allen, C.T., Beidler,
648 J., 2009. Implementation of MOVES-based PM2.5 emissions approach for onroad gasoline
649 sources using hourly, gridded temperatures. 18th Annual International Emission Inventory
650 Conference, Baltimore, MD.

651 Hutzell, W.T., Luecken, D.J., Appel, K.W., Carter, W.P.L., 2011. Interpreting predictions from
652 the SAPRC07 mechanism based on regional and continental simulations. Atmospheric
653 Environment, in press.

654 Jacobson, M.Z., 2007. Effects of Ethanol (E85) versus Gasoline Vehicles on Cancer and
655 Mortality in the United States. Environmental Science & Technology 41, 4150-4157.

656 Jang, J.-C.C., Jeffries, H.E., Tonnesen, S., 1995. Sensitivity of ozone to model grid resolution --
657 II. Detailed process analysis for ozone chemistry. Atmospheric Environment 29, 3101-3114.

658 Jeffries, H.E., 1995. Photochemical Air Pollution, in: Singh, H.B. (Ed.), Composition,
659 Chemistry, and Climate of the Atmosphere. Van Nostrand Reinhold, New York.

660 Jeffries, H.E., Tonnesen, S., 1994. A comparison of two photochemical reaction mechanisms
661 using mass balance and process analysis. Atmospheric Environment 28, 2991-3003.

662 Karst, U., Binding, N., Cammann, K., Witting, U., 1993. Interferences of nitrogen dioxide in the
663 determination of aldehydes and ketones by sampling on 2,4-dinitrophenylhydrazine-coated solid
664 sorbent. Fresenius' Journal of Analytical Chemistry 345, 48-52.

665 Kim, S., Guenther, A., Karl, T., Greenberg, J., 2011. Branch-level measurement of total OH
666 reactivity for constraining unknown BVOC emission during the CABINEX (Community
667 Atmosphere-Biosphere INteractions Experiments)-09 Field Campaign. Atmospheric Chemistry
668 Physics Discussions 11, 7781-7809.

669 Kite, C., 2011. Preliminary comparison between MOVES and MOBILE6
670 Houston/Galveston/Brazoria (HGB) on-road emission inventories for 2006 and 2018. Presented
671 to the Regional Air Quality Planning Committee, Houston, TX.

672 Luecken, D.J., Hutzell, W.T., Gipson, G.L., 2006. Development and analysis of air quality
673 modeling simulations for hazardous air pollutants. Atmospheric Environment 40, 5087-5096.

674 Millet, D.B., Guenther, A., Siegel, D.A., Nelson, N.B., Singh, H.B., de Gouw, J.A., Warneke, C.,
675 Williams, J., Eerdekens, G., Sinha, V., Karl, T., Flocke, F., Apel, E., Riemer, D.D., Palmer, P.I.,
676 Barkley, M., 2010. Global atmospheric budget of acetaldehyde: 3-D model analysis and
677 constraints from in-situ and satellite observations. Atmospheric Chemistry Physics 10, 3405-
678 3425.

679 Millet, D.B., Jacob, D.J., Boersma, K.F., Fu, T.-M., Kurosu, T.P., Chance, K., Heald, C.L.,
680 Guenther, A., 2008. Spatial distribution of isoprene emissions from North America derived from
681 formaldehyde column measurements by the OMI satellite sensor. J. Geophys. Res. 113, D02307.

682 Millet, D.B., Jacob, D.J., Turquety, S., Hudman, R.C., Wu, S., Fried, A., Walega, J., Heikes,
683 B.G., Blake, D.R., Singh, H.B., Anderson, B.E., Clarke, A.D., 2006. Formaldehyde distribution
684 over North America: Implications for satellite retrievals of formaldehyde columns and isoprene
685 emission. Journal of Geophysical Research 111, D24S02.

686 Palmer, P.I., Abbot, D.S., Fu, T.-M., Jacob, D.J., Chance, K., Kurosu, T.P., Guenther, A.,
687 Wiedinmyer, C., Stanton, J.C., Pilling, M.J., Pressley, S.N., Lamb, B., Sumner, A.L., 2006.
688 Quantifying the seasonal and interannual variability of North American isoprene emissions using
689 satellite observations of the formaldehyde column. Journal of Geophysical Research 111,
690 D12315.

691 Paulot, F., Crounse, J.D., Kjaergaard, H.G., Kroll, J.H., Seinfeld, J.H., Wennberg, P.O., 2009.
692 Isoprene photooxidation: new insights into the production of acids and organic nitrates. Atmos.
693 Chemistry Physics 9, 1479-1501.

694 Peeters, J., 2010. HOx radical regeneration in isoprene oxidation via peroxy radical
695 isomerisations. II: experimental evidence and global impact. Physical Chemistry Chemical
696 Physics: PCCP 12, 14227.

697 Rappenglück, B., Dasgupta, P.K., Leuchner, M., Li, Q., Luke, W., 2010. Formaldehyde and its
698 relation to CO, PAN, and SO2 in the Houston-Galveston airshed. Atmospheric Chemistry
699 Physics 10, 2413-2424.

700 Ren, X., Brune, W.H., Mao, J., Mitchell, M.J., Lesher, R.L., Simpas, J.B., Metcalf, A.R.,
701 Schwab, J.J., Cai, C., Li, Y., 2006. Behavior of OH and HO2 in the winter atmosphere in New
702 York City. Atmospheric Environment 40, 252-263.

703 Saunders, S.M., Jenkin, M.E., Derwent, R.G., Pilling, M.J., 2003. Protocol for the development
704 of the Master Chemical Mechanism, MCM v3 (Part A): tropospheric degradation of non-
705 aromatic volatile organic compounds. Atmospheric Chemistry Physics 3, 161-180.

706 Seinfeld, J.H., Pandis, S.N., 1998. Atmospheric Chemistry and Physics. John Wiley & Sons,
707 Inc., New York.

708 Simon, H., Beck, L., Bhave, P., Divita, F., Hsu, Y., Luecken, D., Mobley, D., Pouliot, G., Reff,
709 A., Sarwar, G., Strum, M., 2010. The development and uses of EPA's SPECIATE database.
710 Atmospheric Pollution Research 1, 196-206

711 Sirju, A.-P., Shepson, P.B., 1995. Laboratory and Field Investigation of the DNPH Cartridge
712 Technique for the Measurement of Atmospheric Carbonyl Compounds. Environmental Science
713 & Technology 29, 384-392.

714 Stavrakou, T., Peeters, J., Müller, J.F., 2010. Improved global modelling of HOx recycling in
715 isoprene oxidation: evaluation against the GABRIEL and INTEX-A aircraft campaign
716 measurements. Atmospheric Chemistry Physics 10, 9863-9878.

717 Steiner, A.L., Cohen, R.C., Harley, R.A., Tonse, S., Millet, D.B., Schade, G.W., Goldstein, A.H.,
718 2008. VOC reactivity in central California: comparing an air quality model to ground-based
719 measurements. Atmosmospheric Chemistry Physics 8, 351-368.

720 Sumner, A.L., Shepson, P.B., Couch, T.L., Thornberry, T., Carroll, M.A., Sillman, S., Pippin,
721 M., Bertman, S., Tan, D., Faloona, I., Brune, W., Young, V., Cooper, O., Moody, J., Stockwell,
722 W., 2001. A study of formaldehyde chemistry above a forest canopy. Journal of Geophysical
723 Research 106, 24387-24405.

724 Tilgner, A., Herrmann, H., 2010. Radical-driven carbonyl-to-acid conversion and acid
725 degradation in tropospheric aqueous systems studied by CAPRAM. Atmospheric Environment
726 44, 5415-5422.

727 US EPA, 2010. Renewable Fuel Standard Program (RFS2) Regulatory Impact Analysis,
728 February, 2010 ed. U.S Environmental Protection Agency.

729 US EPA, 2011. 2005 National-Scale Air Toxics Assessment. U.S. Environmental Protection
730 Agency.

731 US GPO, 2011. Code of Federal Requirements, Title 40: Protection of the Environment. US
732 Government Printing Office.

733 Warneck, P., 1989. Sulfur dioxide in rain clouds: Gas-liquid scavenging efficiencies and wet
734 deposition rates in the presence of formaldehyde. Journal of Atmospheric Chemistry 8, 99-117.

735 Warneke, C., de Gouw, J.A., Del Negro, L., Brioude, J., McKeen, S., Stark, H., Kuster, W.C.,
736 Goldan, P.D., Trainer, M., Fehsenfeld, F.C., Wiedinmyer, C., Guenther, A.B., Hansel, A.,
737 Wisthaler, A., Atlas, E., Holloway, J.S., Ryerson, T.B., Peischl, J., Huey, L.G., Hanks, A.T.C.,
738 2010. Biogenic emission measurement and inventories determination of biogenic emissions in
739 the eastern United States and Texas and comparison with biogenic emission inventories. Journal
740 of Geophysical Research 115, D00F18.

741 Warneke, C., McKeen, S.A., de Gouw, J.A., Goldan, P.D., Kuster, W.C., Holloway, J.S.,
742 Williams, E.J., Lerner, B.M., Parrish, D.D., Trainer, M., Fehsenfeld, F.C., Kato, S., Atlas, E.L.,
743 Baker, A., Blake, D.R., 2007. Determination of urban volatile organic compound emission ratios
744 and comparison with an emissions database. Journal of Geophysical Research 112, D10S47.

745 Wert, B.P., Trainer, M., Fried, A., Ryerson, T.B., Henry, B., Potter, W., Angevine, W.M., Atlas,
746 E., Donnelly, S.G., Fehsenfeld, F.C., Frost, G.J., Goldan, P.D., Hansel, A., Holloway, J.S.,
747 Hubler, G., Kuster, W.C., Nicks, D.K., Jr., Neuman, J.A., Parrish, D.D., Schauffler, S., Stutz, J.,
748 Sueper, D.T., Wiedinmyer, C., Wisthaler, A., 2003. Signatures of terminal alkene oxidation in
749 airborne formaldehyde measurements during TexAQS 2000. Journal of Geophysical Research
750 108, 4104.

751 Wiedinmyer, C., Greenberg, J., Guenther, A., Hopkins, B., Baker, K., Geron, C., Palmer, P.I.,
752 Long, B.P., Turner, J.R., Pétron, G., Harley, P., Pierce, T.E., Lamb, B., Westberg, H., Baugh,
753 W., Koerber, M., Janssen, M., 2005. Ozarks Isoprene Experiment (OZIE): Measurements and
754 modeling of the "isoprene volcano". Journal of Geophysical Research 110, D18307.

755 Xie, Y., Elleman, R., Jobson, T., Lamb, B., 2011a. Evaluation of O3-NOx-VOC sensitivities
756 predicted with the CMAQ photochemical model using Pacific Northwest 2001 field
757 observations. Journal of Geophysical Research 116, in press.

758 Xie, Y., Paulot, F., Pinder, R.W., Carter, W.P.L., Nolte, C.G., Luecken, D.J., Hutzell, W.T.,
759 Wennberg, P.O., Cohen, R., 2011b. Understanding the impact of isoprene nitrates and OH
760 reformation on regional air quality using recent advances in isoprene photooxidation chemistry,
761 9th Annual CMAS Conference, Chapel Hill, NC.

762

763

764

Listing of Tables

Listing of Figures

Table 1.

Location	Isoprene		Ethene + Propene		OLE1+OLE2	
	BEIS	MEGAN	BEIS	MEGAN	BEIS	MEGAN
New York	4.4	33.6	1	2.8	1.2	.4
Baltimore	3.5	57.5	.6	5.1	1	.9
Louisville	4.5	12.8	1.2	4.4	1.5	.7
Chicago	19.4	50.3	1	5.2	1.6	.8
Houston	2.9	22.0	1.3	2.9	1.6	.8
Minn	15.9	16.1	2	3.6	2.2	.6
Atlanta	19.1	26.8	2.3	3.7	2.0	.9
Alabama	15.8	53.8	2.3	3.9	3.9	1.4
E. Penn	15.5	41.1	1.5	3.4	1.5	.6
N. Georgia	20.5	34.2	1.5	3.1	1.2	.6

Table 2.

Location	Ethene + Propene		OLE1+OLE2		Pinenes and terpenes	
	January	July	January	July	January	July
New York	.00	.08	.00	.08	.02	.52
Baltimore	.00	.06	.00	.14	.02	.40
Louisville	.00	.16	.01	.24	.04	.65
Chicago	.00	.08	.00	.23	.01	.34
Houston	.12	.35	.10	.31	.55	.82
Minn	.03	.70	.03	.69	.33	.93
Atlanta	.15	.59	.14	.53	.86	.98
Alabama	.07	.82	.45	.91	.99	1.00
E. Penn	.07	.79	.09	.83	.29	.94
N. Georgia	.20	.83	.21	.80	.98	1.00

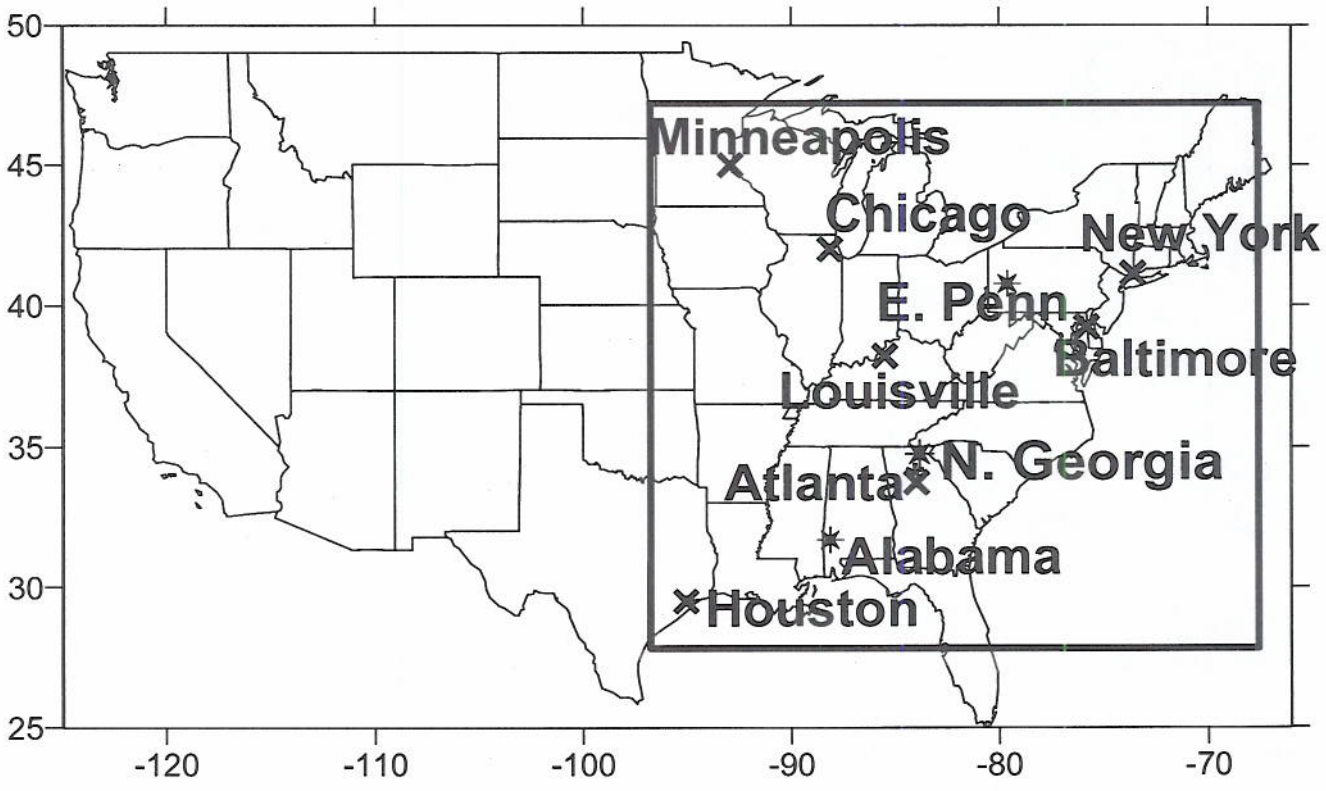
Minneapolis
Chicago
New York
E. Penn
Baltimore
Louisville
N. Georgia
Atlanta
Alabama
Houston
50
45
40
35
30
25
-120
-110
-100
-90
-80
-70

Figure 1.

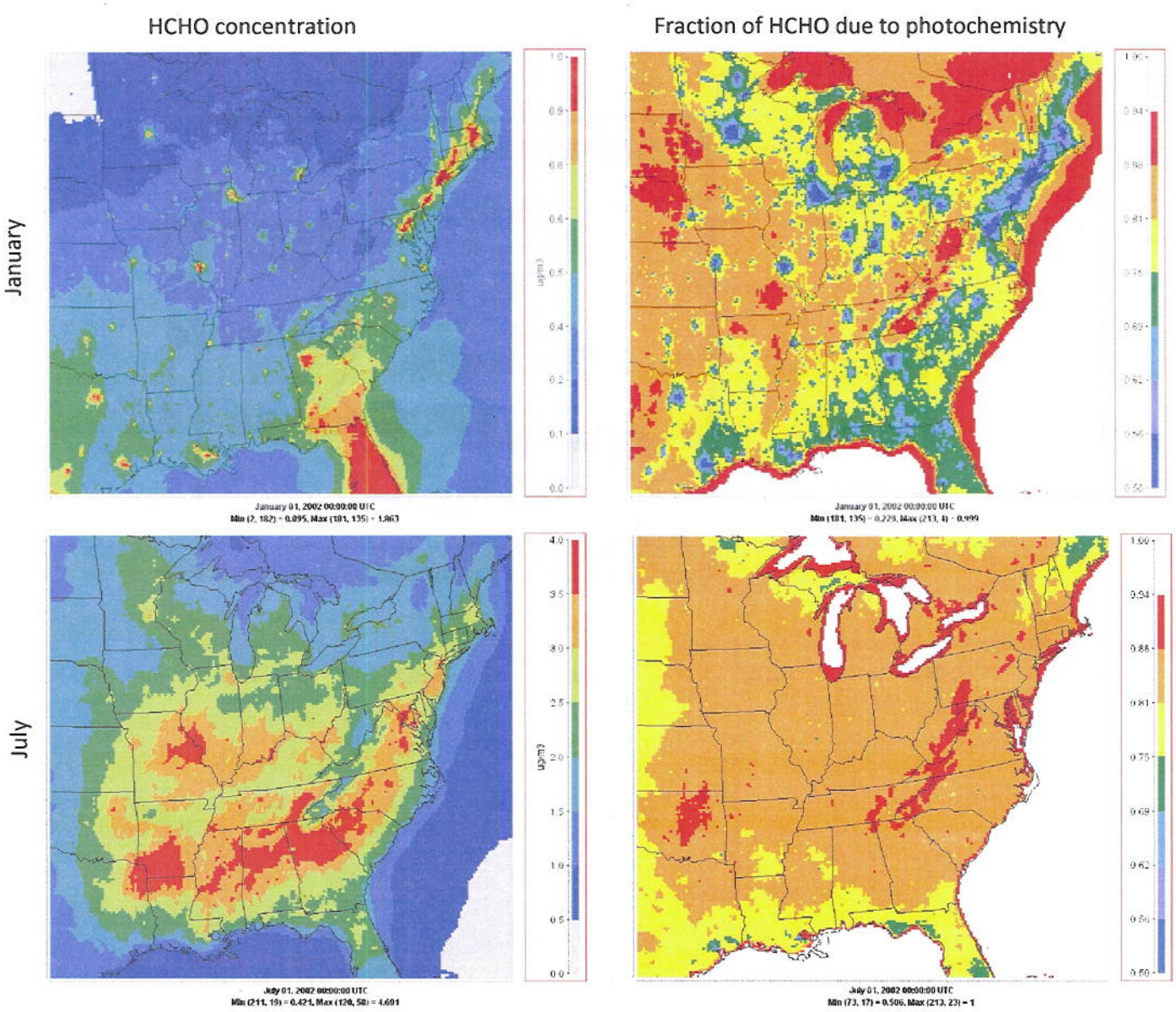
HCHO concentration
Fraction of HCHO due to photochemistry
January
July
ug/m3
January 01, 2002 00:00:00 UTC
July 01, 2002 00:00:00 UTC

Figure 2

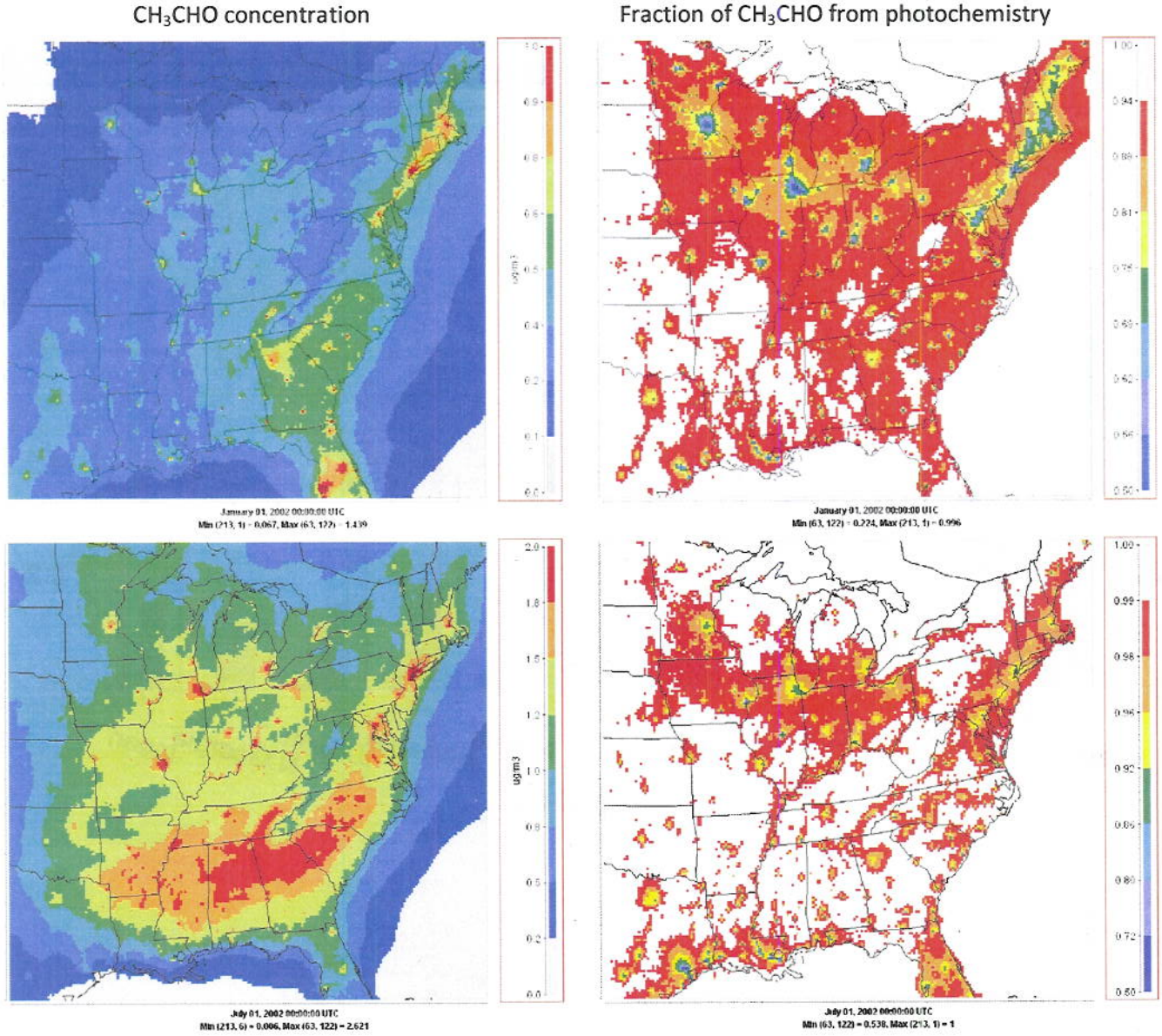
CH3CHO concentration
Fraction of CH3CHO from photochemistry
January
July
ug/m3
January 01, 2002 00:00:00 UTC
Min (213, 1) = 0.067, Max (63, 122) = 1.439
January 01, 2002 00:00:00 UTC
Min (63, 122) = 0.224, Max (213, 1) = 0.996
July 01, 2002 00:00:00 UTC
Min (213, 6) = 0.006, Max (63, 122) = 2.621
July 01, 2002 00:00:00 UTC
Min (63, 122) = 0.538, Max (213, 1) = 1

Figure 3

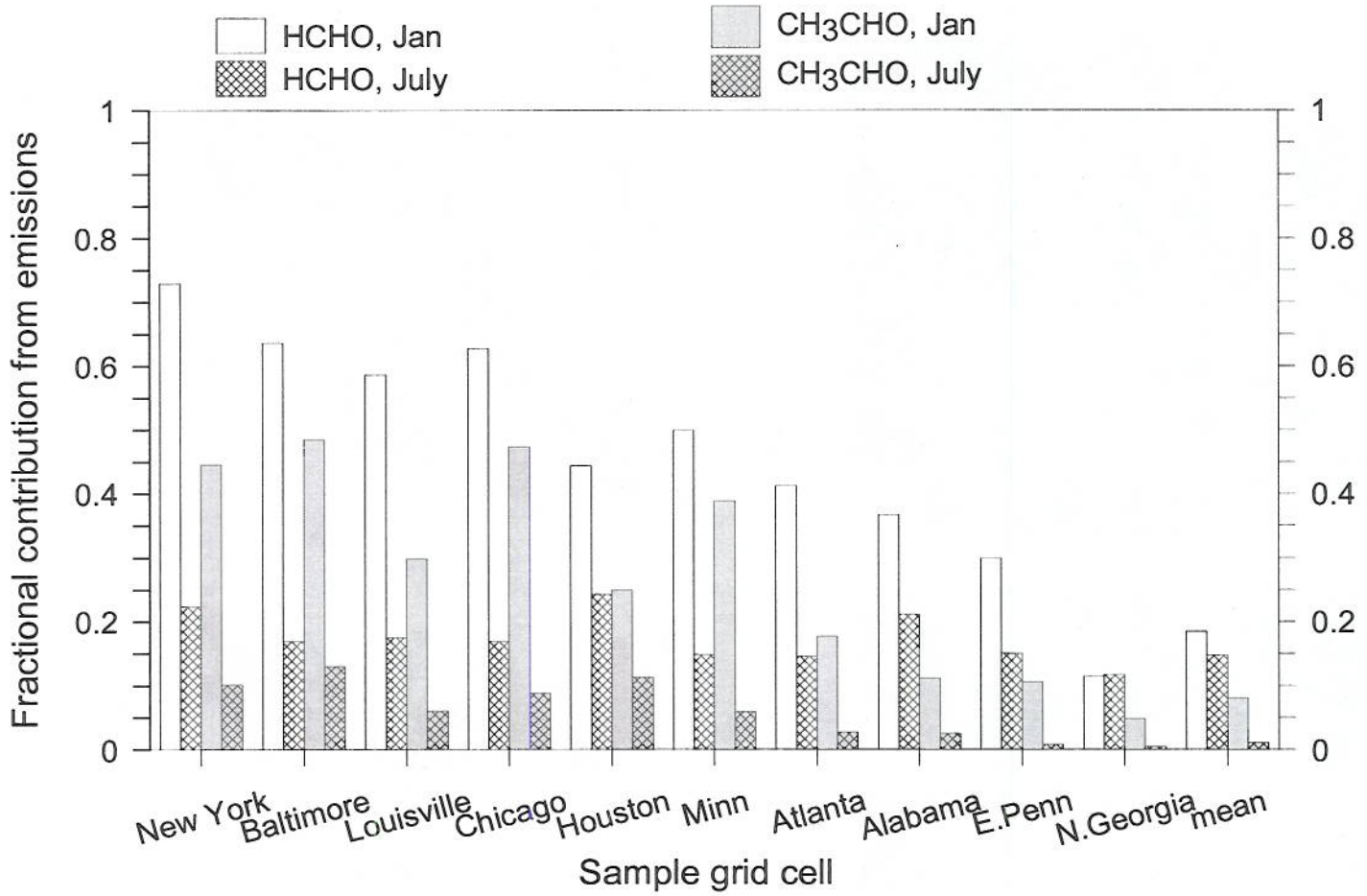
HCHO, Jan
HCHO, July
CH3CHO, Jan
CH3CHO, July
Fractional contribution from emissions
0
0.2
0.4
0.6
0.8
1
New York
Baltimore
Louisville
Chicago
Houston
Minn
Atlanta
Alabama
E.Penn
N.Georgia
mean
Sample grid cell

Figure 4

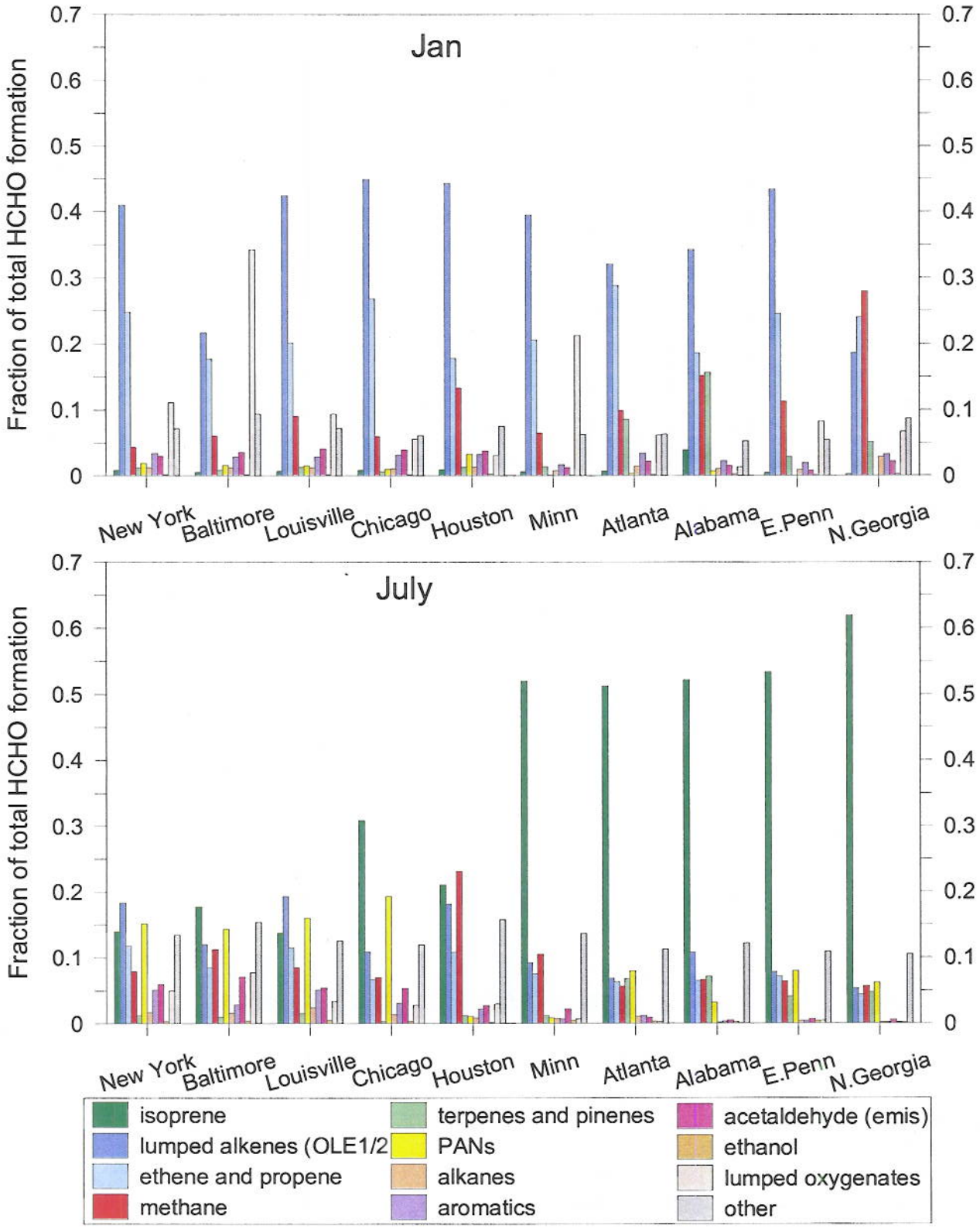
Jan
July
Fraction of total HCHO formation
0.7
0.6
0.5
0.4
0.3
0.2
0.1
0
New York
Baltimore
Louisville
Chicago
Houston
Minn
Atlanta
Alabama
E.Penn
N.Georgia
isoprene
lumped alkenes (OLE1/2
ethene and propene
methane
terpenes and pinenes
PANs
alkanes
aromatics
acetaldehyde (emis)
ethanol
lumped oxygenates
other

Figure 5

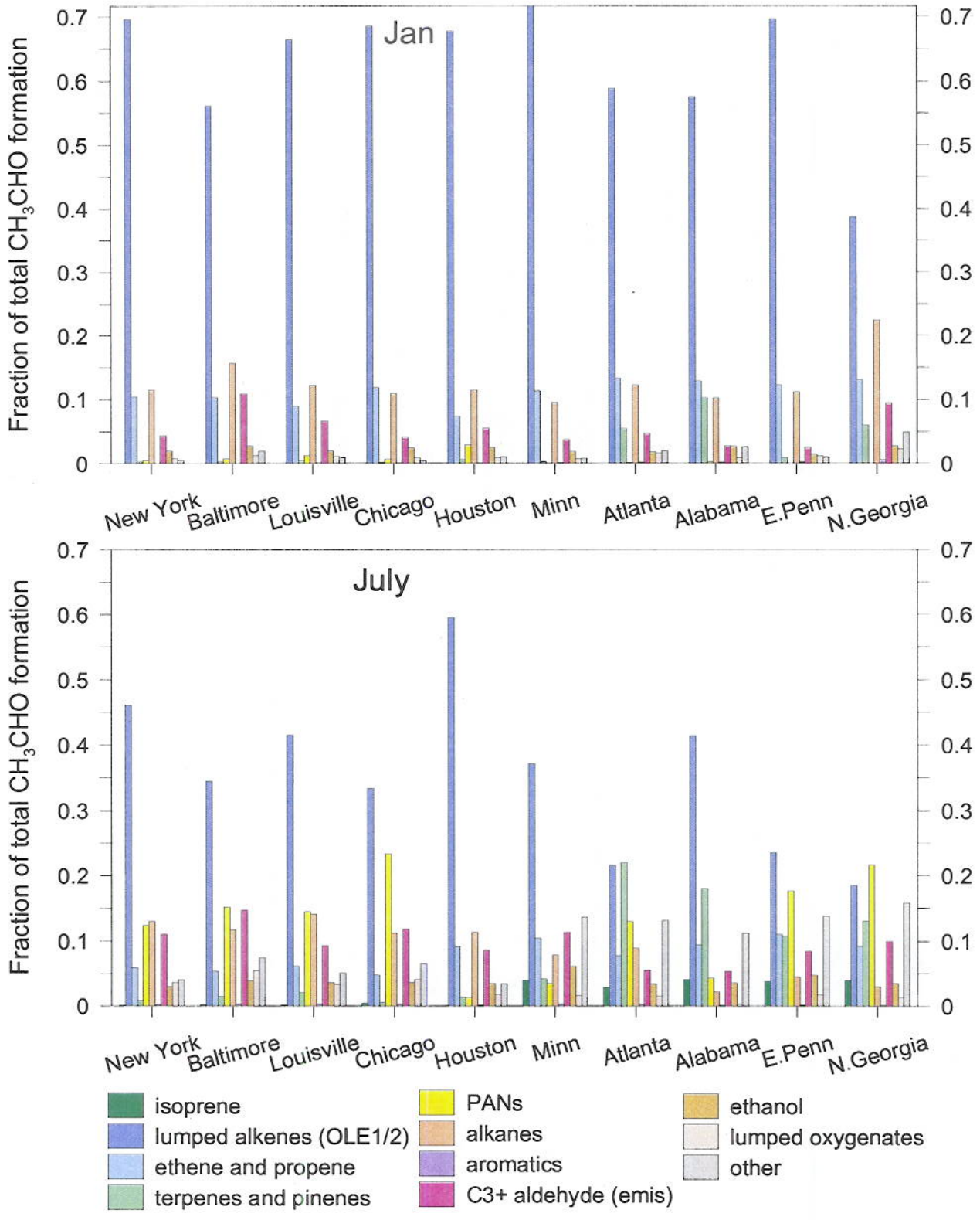
Jan
July
Fraction of total CH_3CHO formation
0
0.1
0.2
0.3
0.4
0.5
0.6
0.7
New York
Baltimore
Louisville
Chicago
Houston
Minn
Atlanta
Alabama
E.Penn
N.Georgia
isoprene
lumped alkenes (OLE1/2)
ethene and propene
terpenes and pinenes
PANs
alkanes
aromatics
C3+ aldehyde (emis)
ethanol
lumped oxygenates
other

Figure 6

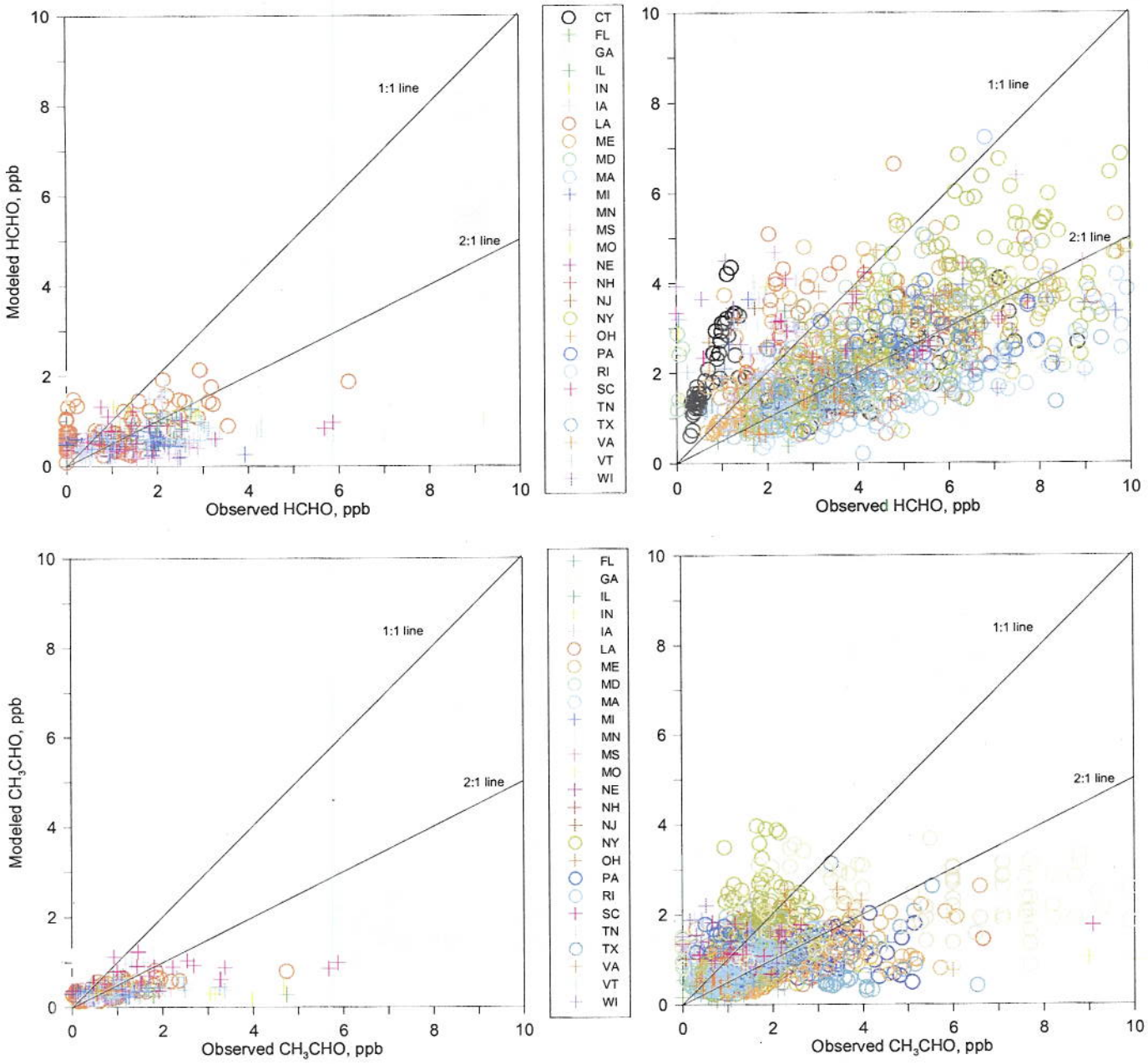
Modeled HCHO, ppb
Observed HCHO, ppb
1:1 line
2:1 line
CT
FL
GA
IL
IN
IA
LA
ME
MD
MA
MI
MN
MS
MO
NE
NH
NJ
NY
OH
PA
RI
SC
TN
TX
VA
VT
WI
Modeled CH3CHO, ppb
Observed CH3CHO, ppb

Figure 7

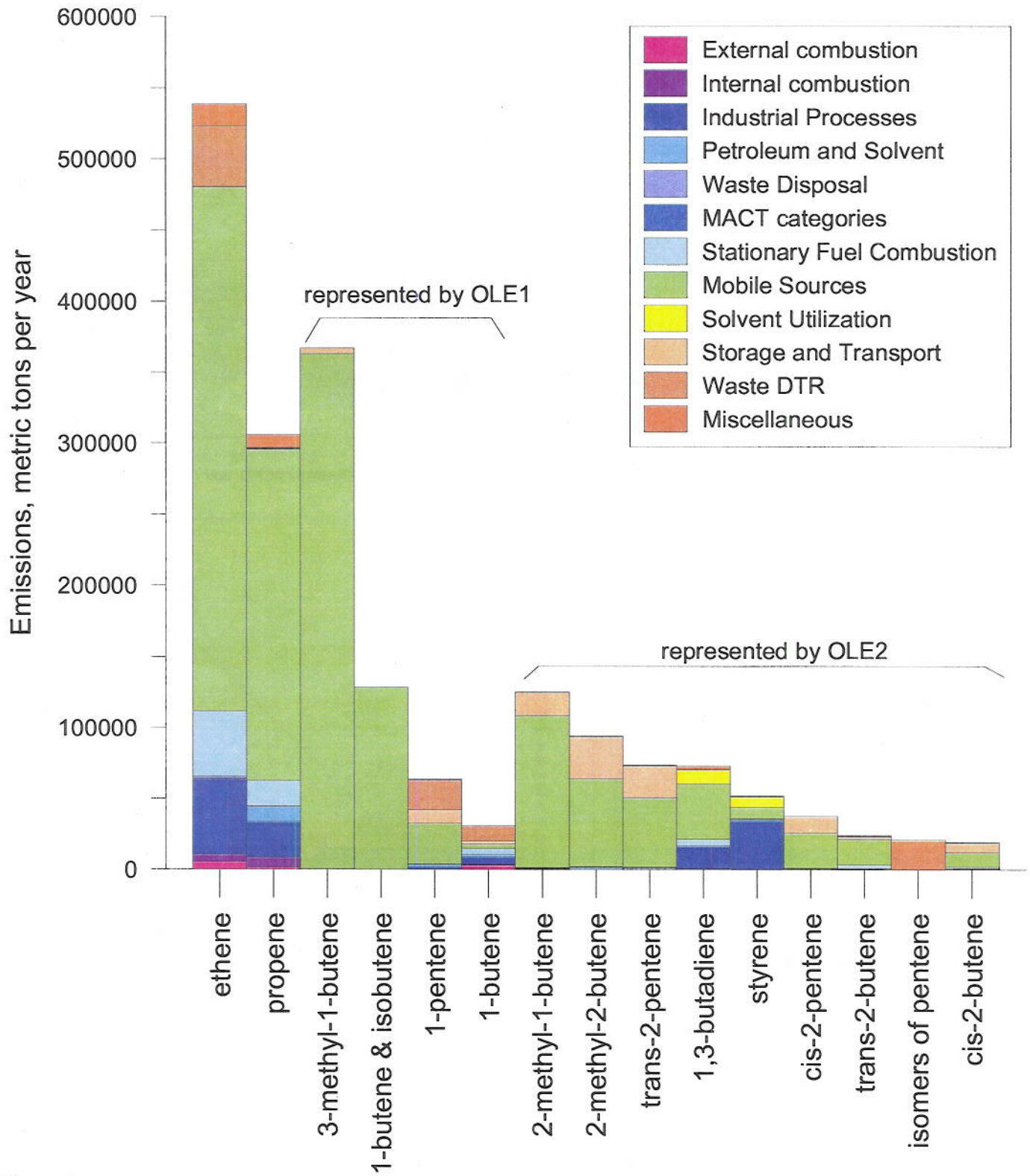
600000
500000
400000
300000
200000
100000
0
Emissions, metric tons per year
External combustion
Internal combustion
Industrial Processes
Petroleum and Solvent
Waste Disposal
MACT categories
Stationary Fuel Combustion
Mobile Sources
Solvent Utilization
Storage and Transport
Waste DTR
Miscellaneous
represented by OLE1
represented by OLE2
ethene
propene
3-methyl-1-butene
1-butene & isobutene
1-pentene
1-butene
2-methyl-1-butene
2-methyl-2-butene
trans-2-pentene
1,3-butadiene
styrene
cis-2-pentene
trans-2-butene
isomers of pentene
cis-2-butene

Figure 8.

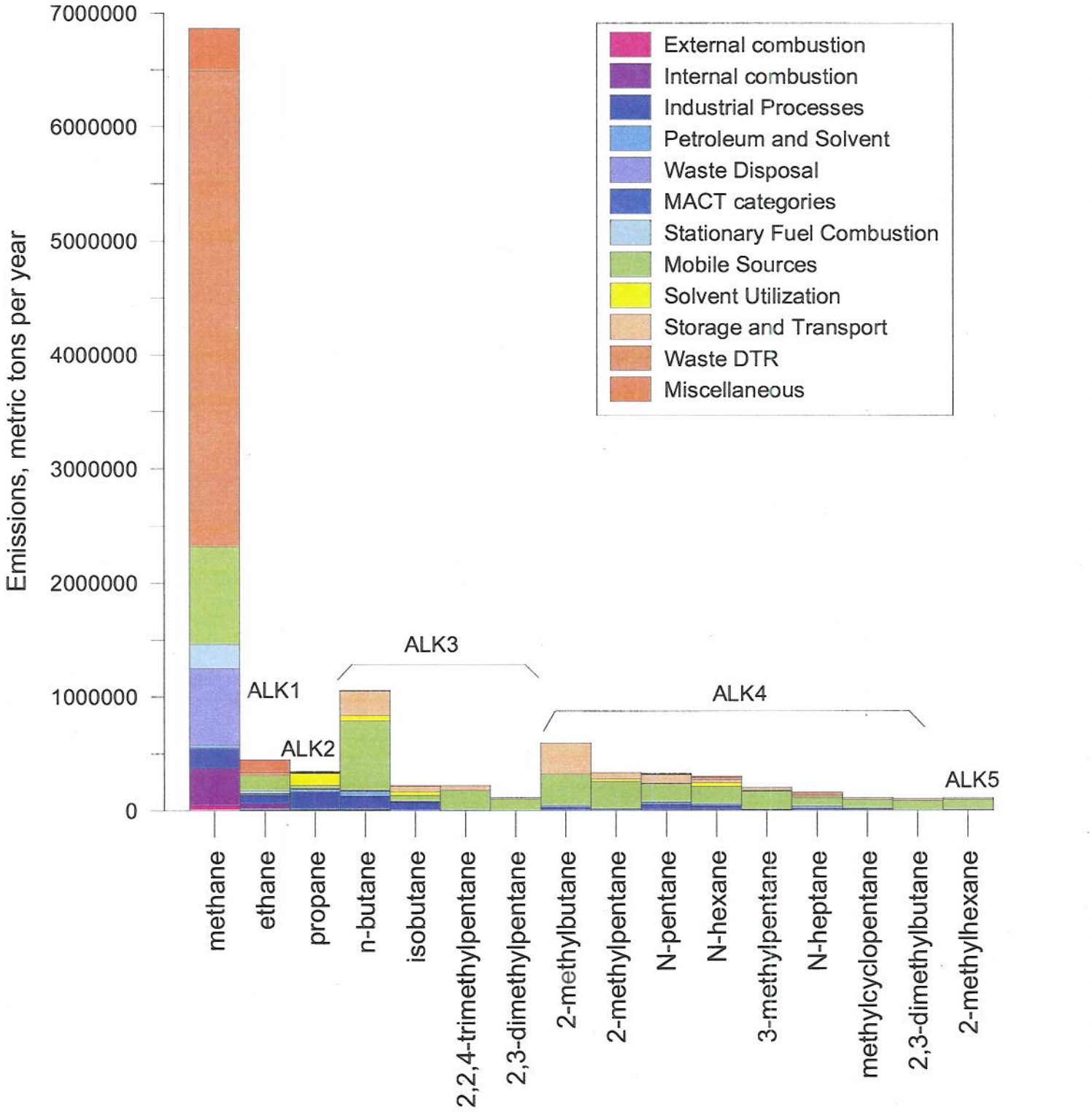

Figure 9: Annual anthropogenic emissions of methane and the highest 15 non-methane alkanes and their allocation by source categories in the NEI. The allocation of explicit species to SAPRC07 model species (ALK1 through ALK5) is also shown.

Table S-1: Listing of reactions that are used in the IRR analysis. Reaction rates and names correspond to those in the entire mechanism, as listed in Hutzell et al., (2010).

Variable Parameter Reaction Rates:

RO2NO = K<BR07>*[NO];
RO2HO2 = K<BR08>*[HO2];
RO2NO3 = K<BR09>*[NO3];
RO2RO2 = K<BR10>*[MEO2]+ K<BR11>*[RO2C] + K<BR11>*[RO2XC];
RO2RO3 = K<BR25>*[MECO3] + K<BR25>*[RCO3] + K<BR25>*[BZCO3] + K<BR25>*[MACO3]
RO2RO= RO2NO+ RO2NO3 + RO2RO3 + 0.5*RO2RO2
RO2XRO = RO2HO2+ 0.5*RO2RO2
RO2RO2M= 0.5*RO2RO2
RO22NN = RO2NO3 + RO2RO3 + 0.5*RO2RO2

name	reactants		products	rate expression
{BR01}	MEO2 + NO	--->	NO2 + HCHO + HO2	k<50> = 2.300E-12 * exp(360.0/T)
{BR02}	MEO2 + HO2	--->	COOH	k<51> = 3.460E-13 * (T/300)**(0.36) * exp(780.0/T)
{BR03}	MEO2 + HO2	--->	HCHO	k<52> = 3.340E-14 * (T/300)**(-3.53) * exp(780.0/T)
{BR04}	MEO2 + NO3	--->	HCHO + HO2 + NO2	k<53> = 1.300E-12
{BR05}	MEO2 + MEO2	--->	MEOH + HCHO	k<54> = 6.390E-14 * (T/300)**(-1.80) * exp(365.0/T)
{BR06}	MEO2 + MEO2	--->	2.000*HCHO +2.000*HO2	k<55> = 7.400E-13 * exp(-520.0/T)
{BR10}	RO2C + MEO2	--->	0.500*HO2 +0.750*HCHO +0.250*MEOH	k<59> = 2.000E-13
{BR15}	RO2XC + MEO2	--->	0.500*HO2 +0.750*HCHO +0.250*MEOH	k<64> = 1.000E+00 * k(BR10)
{BR18}	MECO3 + NO2	--->	PAN	k<67> is a falloff expression using: ko = 2.700E-28 * (T/300)**(-7.10) kinf = 1.210E-11 * (T/300)**(-0.90) F = 0.30, n=1.41
{BR19}	PAN	--->	MECO3 + NO2	k<68> is a falloff expression using: ko = 4.900E-03 * exp(-12100.0/T) kinf = 4.000E+16 * exp(-13600.0/T) F = 0.30, n=1.41
{BR20}	PAN	--hv->	0.600*MECO3 +0.600*NO2 +0.400*MEO2 +0.4*CO2 +0.4*NO3	PAN
{BR21}	MECO3 + NO	--->	MEO2 + CO2 + NO2	k<70> = 7.500E-12 * exp(290.0/T)
{BR22}	MECO3 + HO2	--->	0.700*CCOOOH +0.300*CCOOH +0.300*O3	k<71> = 5.200E-13 * exp(980.0/T)
{BR23}	MECO3 + NO3	--->	MEO2 + CO2 + NO2	k<72> = 1.000E+00 * k(BR09)
{BR24}	MECO3 + MEO2	--->	0.100*CCOOH +0.100*HCHO +0.900*HCHO +0.9*HO2 +0.9*MEO2 +0.9*CO2	k<73> = 2.000E-12 * exp(500.0/T)
{BR25}	MECO3 + RO2C	--->	MEO2 + CO2	k<74> = 4.400E-13 * exp(1070.0/T)
{BR26}	MECO3 + RO2XC	--->	MEO2 + CO2	k<75> = 1.000E+00 * k(BR25)
{BR27}	MECO3 + MECO3	--->	2.000*MEO2 +2.000*CO2	k<76> = 2.900E-12 * exp(500.0/T)
{BR28}	RCO3 + NO2	--->	PAN2	k<77> = 1.210E-11 * (T/300)**(-1.07)
{BR29}	PAN2	--->	RCO3 + NO2	k<78> = 8.300E+16 * exp(-13940.0/T)
{BR30}	PAN2	--hv->	0.600*RCO3 +0.600*NO2 +0.400*RO2C +0.4*xHO2 +0.4*yROOH +0.4*xCCHO +0.4*CO2 +0.4*NO3	PAN
{BR31}	RCO3 + NO	--->	NO2 + RO2C + xHO2 + yROOH + xCCHO + CO2	k<80> = 6.700E-12 * exp(340.0/T)
{BR32}	RCO3 + HO2	--->	0.750*RCOOOH +0.250*RCOOH +0.250*O3	k<81> = 1.000E+00 * k(BR22)
{BR33}	RCO3 + NO3	--->	NO2 + RO2C + xHO2 + yROOH + xCCHO + CO2	k<82> = 1.000E+00 * k(BR09)
{BR34}	RCO3 + MEO2	--->	HCHO + HO2 + RO2C + xHO2 + xCCHO + yROOH + CO2	k<83> = 1.000E+00 * k(BR24)
{BR35}	RCO3 + RO2C	--->	RO2C + xHO2 + xCCHO + yROOH + CO2	k<84> = 1.000E+00 * k(BR25)

{BR36}	RCO3 + RO2XC	--->	RO2C + xHO2 + xCCHO + yROOH + CO2	k<85> = 1.000E+00 * k(BR25)
{BR37}	RCO3 + MECO3	--->	2.000*CO2 + MEO2 + RO2C + xHO2 + yROOH + xCCHO	k<86> = 1.000E+00 * k(BR27)
{BR38}	RCO3 + RCO3	--->	2.000*RO2C +2.000*xHO2 +2.000*xCCHO +2.000*yROOH +2*CO2	k<87> = 1.000E+00 * k(BR27)
{BR39}	BZCO3 + NO2	--->	PBZN	k<88> = 1.370E-11
{BR40}	PBZN	--->	BZCO3 + NO2	k<89> = 7.900E+16 * exp(-14000.0/T)
{BR41}	PBZN	--hv->	0.600*BZCO3 +0.600*NO2 +0.400*CO2 +0.4*BZO +0.4*RO2C +0.4*NO3	PAN
{BR42}	BZCO3 + NO	--->	NO2 + CO2 + BZO + RO2C	k<91> = 1.000E+00 * k(BR31)
{BR43}	BZCO3 + HO2	--->	0.750*RCOOOH +0.250*RCOOH +0.250*O3	k<92> = 1.000E+00 * k(BR22)
{BR44}	BZCO3 + NO3	--->	NO2 + CO2 + BZO + RO2C	k<93> = 1.000E+00 * k(BR09)
{BR45}	BZCO3 + MEO2	--->	HCHO + HO2 + RO2C + BZO + CO2	k<94> = 1.000E+00 * k(BR24)
{BR46}	BZCO3 + RO2C	--->	RO2C + BZO + CO2	k<95> = 1.000E+00 * k(BR25)
{BR47}	BZCO3 + RO2XC	--->	RO2C + BZO + CO2	k<96> = 1.000E+00 * k(BR25)
{BR48}	BZCO3 + MECO3	--->	2.000*CO2 + MEO2 + BZO + RO2C	k<97> = 1.000E+00 * k(BR27)
{BR49}	BZCO3 + RCO3	--->	2.000*CO2 + RO2C + xHO2 + yROOH + xCCHO + BZO + RO2C	k<98> = 1.000E+00 * k(BR27)
{BR50}	BZCO3 + BZCO3	--->	2.000*BZO +2.000*RO2C +2.000*CO2	k<99> = 1.000E+00 * k(BR27)
{BR51}	MACO3 + NO2	--->	MAPAN	k<100> = 1.000E+00 * k(BR28)
{BR52}	MAPAN	--->	MACO3 + NO2	k<101> = 1.600E+16 * exp(-13486.0/T)
{BR53}	MAPAN	--hv->	0.600*MACO3 +0.600*NO2 +0.400*CO2 +0.4*HCHO +0.4*MECO3 +0.4*NO3	PAN
{BR54}	MACO3 + NO	--->	NO2 + CO2 + HCHO + MECO3	k<103> = 1.000E+00 * k(BR31)
{BR55}	MACO3 + HO2	--->	0.750*RCOOOH +0.250*RCOOH +0.250*O3	k<104> = 1.000E+00 * k(BR22)
{BR56}	MACO3 + NO3	--->	NO2 + CO2 + HCHO + MECO3	k<105> = 1.000E+00 * k(BR09)
{BR57}	MACO3 + MEO2	--->	2.000*HCHO + HO2 + CO2 + MECO3	k<106> = 1.000E+00 * k(BR24)
{BR58}	MACO3 + RO2C	--->	CO2 + HCHO + MECO3	k<107> = 1.000E+00 * k(BR25)
{BR59}	MACO3 + RO2XC	--->	CO2 + HCHO + MECO3	k<108> = 1.000E+00 * k(BR25)
{BR60}	MACO3 + MECO3	--->	2.000*CO2 + MEO2 + HCHO + MECO3	k<109> = 1.000E+00 * k(BR27)
{BR61}	MACO3 + RCO3	--->	HCHO + MECO3 + RO2C + xHO2 + yROOH + xCCHO 2*CO2	k<110> = 1.000E+00 * k(BR27)
{BR62}	MACO3 + BZCO3	--->	HCHO + MECO3 + BZO + RO2C +2*CO2	k<111> = 1.000E+00 * k(BR27)
{BR63}	MACO3 + MACO3	--->	2.000*HCHO +2.000*MECO3 +2.000*CO2	k<112> = 1.000E+00 * k(BR27)
{BR64}	TBUO + NO2	--->	RNO3	k<113> = 2.400E-11
{BR65}	TBUO	--->	ACETONE + MEO2	k<114> = 7.500E+14 * exp(-8152.0/T)
{BR66}	BZO + NO2	--->	NPHE	k<115> = 2.300E-11 * exp(150.0/T)
{BR67}	BZO + HO2	--->	CRES	k<116> = 1.000E+00 * k(BR08)
{BR68}	BZO	--->	CRES + RO2C + xHO2	k<117> = 1.000E-03
{RO07}	xMEO2	--->	MEO2	k is variable parameter: RO2RO
{RO08}	xMEO2	--->		k is variable parameter: RO2XRO
{RO09}	xMECO3	--->	MECO3	k is variable parameter: RO2RO
{RO10}	xMECO3	--->		k is variable parameter: RO2XRO
{RO11}	xRCO3	--->	RCO3	k is variable parameter: RO2RO
{RO12}	xRCO3	--->		k is variable parameter: RO2XRO
{RO13}	xMACO3	--->	MACO3	k is variable parameter: RO2RO
{RO14}	xMACO3	--->		k is variable parameter: RO2XRO
{RO15}	xTBUO	--->	TBUO	k is variable parameter: RO2RO
{RO16}	xTBUO	--->		k is variable parameter: RO2XRO

{BP01}	HCHO	--hv->	2.000*HO2 + CO	HCHOR_06
{BP02}	HCHO	--hv->	CO	HCHOM_06
{BP03}	HCHO + OH	--->	HO2 + CO	k<147> = 5.400E-12 * exp(135.0/T)
{BP07}	HCHO + NO3	--->	HNO3 + HO2 + CO	k<148> = 2.000E-12 * exp(-2431.0/T)
{BP08}	CCHO + OH	--->	MECO3	k<149> = 4.400E-12 * exp(365.0/T)
{BP09}	CCHO	--hv->	CO + HO2 + MEO2	CCHO_R
{BP10}	CCHO + NO3	--->	HNO3 + MECO3	k<151> = 1.400E-12 * exp(-1860.0/T)
{BP11}	RCHO + OH	--->	0.965*RCO3 +0.035*RO2C +0.035*xHO2 +0.035*xCO +0.035*xCCHO +0.035*yROOH	k<152> = 5.100E-12 * exp(405.0/T)
{BP12}	RCHO	--hv->	RO2C + xHO2 + yROOH + xCCHO + CO + HO2	C2CHO
{BP13}	RCHO + NO3	--->	HNO3 + RCO3	k<154> = 1.400E-12 * exp(-1601.0/T)
{BP14}	ACETONE + OH	--->	RO2C + xMECO3 + xHCHO + yROOH	k<155> = 4.560E-14 * (T/300)**(3.65) * exp(429.0/T)
{BP15}	ACETONE	--hv->	0.620*MECO3 +1.380*MEO2 +0.380*CO	ACET_06
{BP16}	MEK + OH	--->	0.967*RO2C +0.039*RO2XC +0.039*zRNO3 +0.376*xHO2 +0.51*xMECO3 +0.074*xRCO3 +0.088*xHCHO +0.504*xCCHO +0.376*xRCHO + yROOH	k<157> = 1.300E-12 * (T/300)**(2.00) * exp(-25.0/T)
{BP17}	MEK	--hv->	MECO3 + RO2C + xHO2 + xCCHO + yROOH	
{BP18}	MEOH + OH	--->	HCHO + HO2	k<159> = 2.850E-12 * exp(-345.0/T)
{BP19}	HCOOH + OH	--->	HO2 + CO2	k<160> = 4.500E-13
{BP20}	CCOOH + OH	--->	0.509*MEO2 +0.491*RO2C +0.509*CO2 +0.491*xHO2 +0.491*xMGLY +0.491*yROOH	k<161> = 4.200E-14 * exp(855.0/T)
{BP21}	RCOOH + OH	--->	RO2C + xHO2 +0.143*CO2 +0.142*xCCHO +0.4*xRCHO +0.457*xBACL + yROOH -0.455*XC	k<162> = 1.200E-12
{BP22}	COOH + OH	--->	0.300*HCHO +0.300*OH +0.700*MEO2	k<163> = 3.800E-12 * exp(200.0/T)
{BP23}	COOH	--hv->	HCHO + HO2 + OH	COOH
{BP24}	ROOH + OH	--->	0.744*OH +0.251*RO2C +0.004*RO2XC +0.004*zRNO3 +0.744*RCHO +0.239*xHO2 +0.012*xOH +0.012*xHCHO +0.012*xCCHO +0.205*xRCHO +0.034*xPROD2 +0.256*yROOH	k<165> = 2.500E-11
{BP25}	ROOH	--hv->	RCHO + HO2 + OH	COOH
{BP26}	R6OOH + OH	--->	0.840*OH +0.222*RO2C +0.029*RO2XC +0.029*zRNO3 +0.84*PRD2 +0.09*xHO2 +0.041*xOH +0.02*xCCHO +0.075*xRCHO +0.084*xPROD2 +0.16*yROOH	k<167> = 5.600E-11
{BP27}	R6OOH	--hv->	OH +0.142*HO2 +0.782*RO2C +0.077*RO2XC +0.077*zRNO3 +0.085*RCHO +0.142*PRD2 +0.782*xHO2 +0.026*xCCHO +0.058*xRCHO +0.698*xPROD2 +0.858*yR6OOH	COOH
{BP28}	RAOOH + OH	--->	0.139*OH +0.148*HO2 +0.589*RO2C +0.124*RO2XC +0.124*zRNO3 +0.074*PRD2 +0.147*MGLY +0.139*IPRD +0.565*xHO2 +0.024*xOH +0.448*xRCHO +0.026*xGLY +0.03*xMEK +0.252*xMGLY +0.073*xAFG1 +0.073*xAFG2 +0.713*yR6OOH	k<169> = 1.410E-10
{BP29}	RAOOH	--hv->	OH + HO2 +0.500*GLY +0.5*MGLY +0.5*AFG1 +0.5*AFG2	COOH
{BP30}	GLY	--hv->	2.000*CO +2.000*HO2	GLY_07R
{BP31}	GLY	--hv->	HCHO + CO	GLY_07M
{BP32}	GLY + OH	--->	0.630*HO2 +1.260*CO +0.370*RCO3	k<173> = 1.100E-11
{BP33}	GLY + NO3	--->	HNO3 +0.630*HO2 +1.260*CO +0.37*RCO3	k<174> = 2.800E-12 * exp(-2376.0/T)
{BP34}	MGLY	--hv->	HO2 + CO + MECO3	MGLY_06
{BP35}	MGLY + OH	--->	CO + MECO3	k<176> = 1.500E-11
{BP36}	MGLY + NO3	--->	HNO3 + CO + MECO3	k<177> = 1.400E-12 * exp(-1895.0/T)
{BP37}	BACL	--hv->	2.000*MECO3	BACL_07
{BP38}	CRES + OH	--->	0.200*BZO +0.800*RO2C +0.800*xHO2 +0.8*yR6OOH +0.25*xMGLY	k<179> = 1.700E-12 * exp(950.0/T)

{BP39}	CRES	+ NO3	--->	HNO3 + BZO	k<180> = 1.400E-11
{BP40}	NPHE	+ OH	--->	BZO	k<181> = 3.500E-12
{BP41}	NPHE		--hv->	HONO	1.500E-03 * NO2_06
{BP42}	NPHE		--hv->		1.500E-02 * NO2_06
{BP43}	BALD	+ OH	--->	BZCO3	k<184> = 1.200E-11
{BP44}	BALD		--hv->		6.000E-02 * BALD_06
{BP45}	BALD	+ NO3	--->	HNO3 + BZCO3	k<186> = 1.340E-12 * exp(-1860.0/T)
{BP46}	AFG1	+ OH	--->	0.217*MACO3 +0.723*RO2C +0.060*RO2XC +0.06*zRNO3 +0.521*xHO2 +0.201*xMECO3 +0.334*xCO +0.407*xRCHO +0.129*xMEK +0.107*xGLY +0.267*xMGLY +0.783*yR6OOH	k<187> = 7.400E-11
{BP47}	AFG1	+ O3	--->	0.826*OH +0.522*HO2 +0.652*RO2C +0.522*CO +0.174*CO2 +0.432*GLY +0.568*MGLY +0.652*xRCO3 +0.652*xHCHO +0.652*yR6OOH	k<188> = 9.660E-18
{BP48}	AFG1		--hv->	1.023*HO2 +0.173*MEO2 +0.305*MECO3 +0.5*MACO3 +0.695*CO +0.195*GLY +0.305*MGLY	AFG1
{BP49}	AFG2	+ OH	--->	0.217*MACO3 +0.723*RO2C +0.060*RO2XC +0.06*zRNO3 +0.521*xHO2 +0.201*xMECO3 +0.334*xCO +0.407*xRCHO +0.129*xMEK +0.107*xGLY +0.267*xMGLY +0.783*yR6OOH	k<190> = 7.400E-11
{BP50}	AFG2	+ O3	--->	0.826*OH +0.522*HO2 +0.652*RO2C +0.522*CO +0.174*CO2 +0.432*GLY +0.568*MGLY +0.652*xRCO3 +0.652*xHCHO +0.652*yR6OOH	k<191> = 9.660E-18
{BP51}	AFG2		--hv->	PRD2	AFG1
{BP52}	AFG3	+ OH	--->	0.206*MACO3 +0.733*RO2C +0.117*RO2XC +0.117*zRNO3 +0.561*xHO2 +0.117*xMECO3 +0.114*xCO +0.274*xGLY +0.153*xMGLY +0.019*xBACL +0.195*xAFG1 +0.195*xAFG2 +0.231*xIPRD +0.794*yR6OOH	k<193> = 9.350E-11
{BP53}	AFG3	+ O3	--->	0.471*OH +0.554*HO2 +0.013*MECO3 +0.258*RO2C +0.007*RO2XC +0.007*zRNO3 +0.58*CO +0.19*CO2 +0.366*GLY +0.184*MGLY +0.35*AFG1 +0.35*AFG2 +0.139*AFG3 +0.003*MACR +0.004*MVK +0.003*IPRD +0.095*xHO2 +0.163*xRCO3	k<194> = 1.430E-17
{BP54}	MACR	+ OH	--->	0.500*MACO3 +0.500*RO2C +0.500*xHO2 +0.416*xCO +0.084*xHCHO +0.416*xMEK +0.084*xMGLY +0.5*yROOH	k<195> = 8.000E-12 * exp(380.0/T)
{BP55}	MACR	+ O3	--->	0.208*OH +0.108*HO2 +0.100*RO2C +0.45*CO +0.117*CO2 +0.1*HCHO +0.9*MGLY +0.333*HCOOH +0.1*xRCO3 +0.1*xHCHO +0.1*yROOH	k<196> = 1.400E-15 * exp(-2100.0/T)
{BP56}	MACR	+ NO3	--->	0.500*MACO3 +0.500*RO2C +0.500*HNO3 +0.5*xHO2 +0.5*xCO +0.5*yROOH	k<197> = 1.500E-12 * exp(-1815.0/T)
{BP57}	MACR	+ O3P	--->	RCHO	k<198> = 6.340E-12
{BP58}	MACR		--hv->	0.330*OH +0.670*HO2 +0.340*MECO3 +0.33*MACO3 +0.33*RO2C +0.67*CO +0.34*HCHO +0.33*xMECO3 +0.33*xHCHO +0.33*yROOH	MACR_06
{BP59}	MVK	+ OH	--->	0.975*RO2C +0.025*RO2XC +0.025*zRNO3 +0.3*xHO2 +0.675*xMECO3 +0.3*xHCHO +0.675*xHOCCHO +0.3*xMGLY + yROOH	k<200> = 2.600E-12 * exp(610.0/T)
{BP60}	MVK	+ O3	--->	0.164*OH +0.064*HO2 +0.050*RO2C +0.05*xHO2 +0.475*CO +0.124*CO2 +0.05*HCHO +0.95*MGLY +0.351*HCOOH +0.05*xRCO3 +0.05*xHCHO +0.05*yROOH	k<201> = 8.500E-16 * exp(-1520.0/T)
{BP62}	MVK	+ O3P	--->	0.450*RCHO +0.550*MEK	k<202> = 4.320E-12

{BP63}	MVK	--hv->	0.400*MEO2 +0.600*CO +0.600*PRD2 +0.4*MACO3	MVK_06
{BP64}	IPRD + OH	--->	0.289*MACO3 +0.670*RO2C +0.670*xHO2 +0.041*RO2XC +0.041*zRNO3 +0.336*xCO +0.055*xHCHO +0.129*xHOCCHO +0.013*xRCHO +0.15*xMEK +0.332*xPROD2 +0.15*xGLY +0.174*xMGLY +0.711*yR6OOH	k<204> = 6.190E-11
{BP65}	IPRD + O3	--->	0.285*OH +0.400*HO2 +0.048*RO2C +0.048*xRCO3 +0.498*CO +0.14*CO2 +0.124*HCHO +0.21*MEK +0.023*GLY +0.742*MGLY +0.1*HCOOH +0.372*RCOOH +0.047*xHOCCHO +0.001*xHCHO +0.048*yR6OOH	k<205> = 4.180E-18
{BP66}	IPRD + NO3	--->	0.150*MACO3 +0.150*HNO3 +0.799*RO2C +0.799*xHO2 +0.051*RO2XC +0.051*zRNO3 +0.572*xCO +0.227*xHCHO +0.218*xRCHO +0.008*xMGLY +0.572*xRNO3 +0.85*yR6OOH	k<206> = 1.000E-13
{BP67}	IPRD	--hv->	1.233*HO2 +0.467*MECO3 +0.300*RCO3 +1.233*CO +0.3*HCHO +0.467*HOCCHO +0.233*MEK	MACR_06
{BP68}	PRD2 + OH	--->	0.472*HO2 +0.379*xHO2 +0.029*xMECO3 +0.049*xRCO3 +0.473*RO2C +0.071*RO2XC +0.071*zRNO3 +0.002*HCHO +0.211*xHCHO +0.001*CCHO +0.083*xCCHO +0.143*RCHO +0.402*xRCHO +0.115*xMEK +0.329*PRD2 +0.007*xPROD2 +0.528*yR6OOH	k<208> = 1.550E-11
{BP69}	PRD2	--hv->	0.913*xHO2 +0.400*MECO3 +0.600*RCO3 +1.59*RO2C +0.087*RO2XC +0.087*zRNO3 +0.303*xHCHO +0.163*xCCHO +0.78*xRCHO + yR6OOH	4.860E-03*MEK_06
{BP70}	RNO3 + OH	--->	0.189*HO2 +0.305*xHO2 +0.019*NO2 +0.313*xNO2 +0.976*RO2C +0.175*RO2XC +0.175*zRNO3 +0.011*xHCHO +0.429*xCCHO +0.001*RCHO +0.036*xRCHO +0.004*xACETONE +0.01*MEK +0.17*xMEK +0.008*PRD2 +0.031*xPROD2 +0.189*RNO3 +0.305*xRNO3	k<210> = 7.200E-12
{BP71}	RNO3	--hv->	0.344*HO2 +0.554*xHO2 + NO2 +0.721*RO2C +0.102*RO2XC +0.102*zRNO3 +0.074*HCHO +0.061*xHCHO +0.214*CCHO +0.23*xCCHO +0.074*RCHO +0.063*xRCHO +0.008*xACETONE +0.124*MEK +0.083*xMEK +0.19*PRD2 +0.261*xPROD2 +0.066*yROOH	IC3ONO2
{BP72}	HOCCHO + OH	--->	MECO3	k<212> = 1.000E+00 * k(BP08)
{BP73}	HOCCHO	--hv->	CO +2.000*HO2 + HCHO	HOCCHO_IUPAC
{BP74}	HOCCHO + NO3	--->	HNO3 + MECO3	k<214> = 1.000E+00 * k(BP10)
{BP75}	ACROLEIN + OH	--->	0.250*xHO2 +0.750*MACO3 +0.250*RO2C +0.167*xCO +0.083*xHCHO +0.167*xCCHO +0.083*xGLY +0.25*yROOH -0.75*XC	k<215> = 1.990E-11
{BP76}	ACROLEIN + O3	--->	0.830*HO2 +0.330*OH +1.005*CO +0.31*CO2 +0.5*HCHO +0.185*HCOOH +0.5*GLY	k<216> = 1.400E-15 * exp(-2528.0/T)
{BP77}	ACROLEIN + NO3	--->	0.031*xHO2 +0.967*MACO3 +0.031*RO2C +0.002*RO2XC +0.002*zRNO3 +0.967*HNO3 +0.031*xCO +0.031*xRNO3 +0.033*yROOH	k<217> = 1.180E-15
{BP78}	ACROLEIN + O3P	--->	RCHO	k<218> = 2.370E-12
{BP79}	ACROLEIN	--hv->	1.066*HO2 +0.178*OH +0.234*MEO2 +0.33*MACO3 +1.188*CO +0.102*CO2 +0.34*HCHO +0.05*CCOOH -0.284*XC	ACRO_09
{BP80}	CCOOOH + OH	--->	0.980*MECO3 +0.020*RO2C +0.020*CO2 +0.02*xOH +0.02*xHCHO +0.02*yROOH	k<220> = 5.280E-12
{BP81}	CCOOOH	--hv->	MEO2 + CO2 + OH	PAA
{BP82}	RCOOOH + OH	--->	0.806*RCO3 +0.194*RO2C +0.194*yROOH +0.11*CO2 +0.11*xOH +0.11*xCCHO +0.084*xHO2 +0.084*xRCHO	k<222> = 6.420E-12

{BP83}	RCOOOH	--hν->	xHO2 + xCCHO + yROOH + CO2 + OH	PAA
{PO01}	xHCHO	--->	HCHO	k is variable parameter: RO2RO
{PO02}	xHCHO	--->		k is variable parameter: RO2XRO
{PO03}	xCCHO	--->	CCHO	k is variable parameter: RO2RO
{PO04}	xCCHO	--->		k is variable parameter: RO2XRO
{PO05}	xRCHO	--->	RCHO	k is variable parameter: RO2RO
{PO06}	xRCHO	--->		k is variable parameter: RO2XRO
{PO07}	xACETONE	--->	ACETONE	k is variable parameter: RO2RO
{PO08}	xACETONE	--->		k is variable parameter: RO2XRO
{PO09}	xMEK	--->	MEK	k is variable parameter: RO2RO
{PO10}	xMEK	--->		k is variable parameter: RO2XRO
{PO11}	xPROD2	--->	PRD2	k is variable parameter: RO2RO
{PO12}	xPROD2	--->		k is variable parameter: RO2XRO
{PO13}	xGLY	--->	GLY	k is variable parameter: RO2RO
{PO14}	xGLY	--->		k is variable parameter: RO2XRO
{PO15}	xMGLY	--->	MGLY	k is variable parameter: RO2RO
{PO16}	xMGLY	--->		k is variable parameter: RO2XRO
{PO17}	xBACL	--->	BACL	k is variable parameter: RO2RO
{PO18}	xBACL	--->		k is variable parameter: RO2XRO
{PO19}	xBALD	--->	BALD	k is variable parameter: RO2RO
{PO20}	xBALD	--->		k is variable parameter: RO2XRO
{PO21}	xAFG1	--->	AFG1	k is variable parameter: RO2RO
{PO22}	xAFG1	--->		k is variable parameter: RO2XRO
{PO23}	xAFG2	--->	AFG2	k is variable parameter: RO2RO
{PO24}	xAFG2	--->		k is variable parameter: RO2XRO
{PO25}	xAFG3	--->	AFG3	k is variable parameter: RO2RO
{PO26}	xAFG3	--->		k is variable parameter: RO2XRO
{PO27}	xMACR	--->	MACR	k is variable parameter: RO2RO
{PO28}	xMACR	--->		k is variable parameter: RO2XRO
{PO29}	xMVK	--->	MVK	k is variable parameter: RO2RO
{PO30}	xMVK	--->		k is variable parameter: RO2XRO
{PO31}	xIPRD	--->	IPRD	k is variable parameter: RO2RO
{PO32}	xIPRD	--->		k is variable parameter: RO2XRO
{PO33}	xRNO3	--->	RNO3	k is variable parameter: RO2RO
{PO34}	xRNO3	--->		k is variable parameter: RO2XRO
{PO35}	zRNO3	--->	RNO3	k is variable parameter: RO2NO
{PO36}	zRNO3	--->	PRD2 + HO2	k is variable parameter: RO22NN
{PO37}	zRNO3	--->		k is variable parameter: RO2XRO
{PO38}	yROOH	--->	ROOH	k is variable parameter: RO2HO2
{PO39}	yROOH	--->	MEK	k is variable parameter: RO2RO2M
{PO40}	yROOH	--->		k is variable parameter: RO2RO
{PO41}	yR6OOH	--->	R6OOH	k is variable parameter: RO2HO2
{PO42}	yR6OOH	--->	PRD2	k is variable parameter: RO2RO2M
{PO43}	yR6OOH	--->		k is variable parameter: RO2RO
{PO44}	yRAOOH	--->	RAOOH	k is variable parameter: RO2HO2
{PO45}	yRAOOH	--->	PRD2	k is variable parameter: RO2RO2M
{PO46}	yRAOOH	--->		k is variable parameter: RO2RO
{PO47}	xHOCCHO	--->	HOCCHO	k is variable parameter: RO2RO
{PO48}	xHOCCHO	--->		k is variable parameter: RO2XRO
{PO49}	xACROLEIN	--->	ACROLEIN	k is variable parameter: RO2RO
{PO50}	xACROLEIN	--->		k is variable parameter: RO2XRO
{BE01}	CH4 + OH	--->	MEO2	k<274>= 1.850E-12 * exp(-1690.0/T)
{BE02}	ETHENE + OH	--->	xHO2 + RO2C +1.610*xHCHO +0.195*xHOCCHO + yROOH	k<275> is a falloff expression using: ko = 1.000E-28 * (T/300)**(-4.50) kinf = 8.800E-12 * (T/300)**(-0.85) F = 0.60, n=1.00
{BE03}	ETHENE + O3	--->	0.160*HO2 +0.160*OH +0.510*CO +0.12*CO2 + HCHO +0.37*HCOOH	k<276>= 9.140E-15 * exp(-2580.0/T)
{BE04}	ETHENE + NO3	--->	xHO2 + RO2C + xRCHO + yROOH	k<277>= 3.300E-12 * (T/300)**(2.00) * exp(-2880.0/T)
{BE05}	ETHENE + O3P	--->	0.800*HO2 +0.290*xHO2 +0.510*MEO2 +0.29*RO2C +0.51*CO +0.278*xCO +0.278*xHCHO +0.1*CCHO +0.012*xGLY +0.29*yROOH	k<278>= 1.070E-11 * exp(-800.0/T)

{BT01}	PROPENE + OH --->	0.984*xHO2 +0.984*RO2C +0.016*RO2XC +0.016*zRNO3 +0.984*xHCHO +0.984*xCCHO + yROOH	k<279> = 4.850E-12 * exp(504.0/T)
{BT02}	PROPENE + O3 --->	0.165*HO2 +0.350*OH +0.355*MEO2 +0.525*CO +0.215*CO2 +0.5*HCHO +0.5*CCHO +0.185*HCOOH +0.075*CCOOH	k<280> = 5.510E-15 * exp(-1878.0/T)
{BT03}	PROPENE + NO3 --->	0.949*xHO2 +0.949*RO2C +0.051*RO2XC +0.051*zRNO3 + yROOH	k<281> = 4.590E-13 * exp(-1156.0/T)
{BT04}	PROPENE + O3P --->	0.450*RCHO +0.550*MEK	k<282> = 1.020E-11 * exp(-280.0/T)
{BT05}	BUTADIENE13 + OH --->	0.951*xHO2 +1.189*RO2C +0.049*RO2XC +0.049*zRNO3 +0.708*xHCHO +0.48*xACROLEIN +0.471*xIPRD + yROOH	k<283> = 1.480E-11 * exp(448.0/T)
{BT06}	BUTADIENE13 + O3 --->	0.080*HO2 +0.080*OH +0.255*CO +0.185*CO2 +0.5*HCHO +0.185*HCOOH +0.5*ACROLEIN +0.375*MVK +0.125*PRD2	k<284> = 1.340E-14 * exp(-2283.0/T)
{BT07}	BUTADIENE13 + NO3 --->	0.815*xHO2 +0.120*xNO2 +1.055*RO2C +0.065*RO2XC +0.065*zRNO3 +0.115*xHCHO +0.46*xMVK +0.12*xIPRD +0.355*xRNO3 + yROOH	k<285> = 1.000E-13
{BT08}	BUTADIENE13 + O3P --->	0.250*HO2 +0.117*xHO2 +0.118*xMACO3 +0.235*RO2C +0.015*RO2XC +0.015*zRNO3 +0.115*xCO +0.115*xACROLEIN +0.001*xAFG1 +0.001*xAFG2 +0.75*PRD2 +0.25*yROOH	k<286> = 2.260E-11 * exp(-40.0/T)
{BE06}	ISOPRENE + OH --->	0.907*xHO2 +0.986*RO2C +0.093*RO2XC +0.093*zRNO3 +0.624*xHCHO +0.23*xMACR +0.32*xMVK +0.357*xIPRD + yR6OOH + ISOPRXN	k<287> = 2.540E-11 * exp(410.0/T)
{BE07}	ISOPRENE + O3 --->	0.066*HO2 +0.266*OH +0.192*xMACO3 +0.192*RO2C +0.008*RO2XC +0.008*zRNO3 +0.275*CO +0.122*CO2 +0.4*HCHO +0.192*xHCHO +0.204*HCOOH +0.39*MACR +0.16*MVK +0.15*IPRD +0.1*PRD2 +0.2*yR6OOH	k<288> = 7.860E-15 * exp(-1912.0/T)
{BE08}	ISOPRENE + NO3 --->	0.749*xHO2 +0.187*xNO2 +0.936*RO2C +0.064*RO2XC +0.064*zRNO3 +0.936*xIPRD + yR6OOH	k<289> = 3.030E-12 * exp(-448.0/T)
{BE09}	ISOPRENE + O3P --->	0.250*MEO2 +0.240*xMACO3 +0.240*RO2C +0.01*RO2XC +0.01*zRNO3 +0.24*xHCHO +0.75*PRD2 +0.25*yR6OOH	k<290> = 3.500E-11
{BT09}	APIN + OH --->	0.799*xHO2 +0.004*xRCO3 +1.042*RO2C +0.197*RO2XC +0.197*zRNO3 +0.002*xCO +0.022*xHCHO +0.776*xRCHO +0.034*xACETONE +0.02*xMGLY +0.023*xBACL + yR6OOH + TRPRXN	k<291> = 1.210E-11 * exp(436.0/T)
{BT10}	APIN + O3 --->	0.009*HO2 +0.102*xHO2 +0.728*OH +0.001*xMECO3 +0.297*xRCO3 +1.511*RO2C +0.337*RO2XC +0.337*zRNO3 +0.029*CO +0.051*xCO +0.017*CO2 +0.344*xHCHO +0.24*xRCHO +0.345*xACETONE +0.008*MEK +0.002*xGLY +0.081*xBACL +0.255*PRD2	k<292> = 5.000E-16 * exp(-530.0/T)
{BT11}	APIN + NO3 --->	0.056*HO2 +0.643*xNO2 +0.007*xRCO3 +1.05*RO2C +0.293*RO2XC +0.293*zRNO3 +0.005*xCO +0.007*xHCHO +0.684*xRCHO +0.069*xACETONE +0.002*xMGLY +0.056*xRNO3 + yR6OOH + TRPRXN	k<293> = 1.190E-12 * exp(490.0/T)
{BT12}	APIN + O3P --->	PRD2 + TRPRXN	k<294> = 3.200E-11
{BE10}	ACETYLENE + OH --->	0.300*HO2 +0.700*OH +0.300*CO +0.3*HCOOH +0.7*GLY	k<295> is a falloff expression using: ko = 5.500E-30 * (T/300)**(-2.00) kinf = 8.300E-13 F = 0.60, n=1.00
{BE11}	ACETYLENE + O3 --->	1.500*HO2 +0.500*OH +1.500*CO +0.5*CO2	k<296> = 1.000E-14 * exp(-4100.0/T)

{BE12}	BENZENE + OH	--->	0.570*HO2 +0.290*xHO2 +0.116*OH +0.29*RO2C +0.024*RO2XC +0.024*zRNO3 +0.29*xGLY +0.57*CRES +0.029*xAFG1 +0.261*xAFG2 +0.116*AFG3 +0.314*yRAOOH + BENZRO2	k<297>= 2.330E-12 * exp(-193.0/T)
{BT13}	TOLUENE + OH	--->	0.181*HO2 +0.454*xHO2 +0.312*OH +0.454*RO2C +0.054*RO2XC +0.054*zRNO3 +0.238*xGLY +0.151*xMGLY +0.181*CRES +0.065*xBALD +0.195*xAFG1 +0.195*xAFG2 +0.312*AFG3 +0.073*yR6OOH +0.435*yRAOOH + TOLRO2	k<298>= 1.810E-12 * exp(338.0/T)
{BT14}	MXYL + OH	--->	0.159*HO2 +0.520*xHO2 +0.239*OH +0.52*RO2C +0.082*RO2XC +0.082*zRNO3 +0.1*xGLY +0.38*xMGLY +0.159*CRES +0.041*xBALD +0.336*xAFG1 +0.144*xAFG2 +0.239*AFG3 +0.047*yR6OOH +0.555*yRAOOH + XYLRO2	k<299>= 2.310E-11
{BT15}	OXYL + OH	--->	0.161*HO2 +0.554*xHO2 +0.198*OH +0.554*RO2C +0.087*RO2XC +0.087*zRNO3 +0.084*xGLY +0.238*xMGLY +0.185*xBACL +0.161*CRES +0.047*xBALD +0.253*xAFG1 +0.253*xAFG2 +0.198*AFG3 +0.055*yR6OOH +0.586*yRAOOH + XYLRO2	k<300>= 1.360E-11
{BT16}	PXYL + OH	--->	0.159*HO2 +0.487*xHO2 +0.278*OH +0.487*RO2C +0.076*RO2XC +0.076*zRNO3 +0.286*xGLY +0.112*xMGLY +0.159*CRES +0.088*xBALD +0.045*xAFG1 +0.067*xAFG2 +0.278*AFG3 +0.286*xAFG3 +0.102*yR6OOH +0.461*yRAOOH + XYLRO2	k<301>= 1.430E-11
{BT17}	TRIMETH_BENZ + OH	--->	0.022*HO2 +0.627*xHO2 +0.230*OH +0.627*RO2C +0.121*RO2XC +0.121*zRNO3 +0.074*xGLY +0.405*xMGLY +0.112*xBACL +0.022*CRES +0.036*xBALD +0.088*xAFG1 +0.352*xAFG2 +0.23*AFG3 +0.151*xAFG3 +0.043*yR6OOH +0.705*yRAOOH + XYLRO2	k<302>= 3.250E-11
{BT18}	ETOH + OH	--->	0.950*HO2 +0.050*xHO2 +0.050*RO2C +0.081*xHCHO +0.95*CCHO +0.01*xHOCCHO +0.05*yROOH	k<303>= 5.490E-13 * (T/300)**(2.00) * exp(530.0/T)
{BL01}	ALK1 + OH	--->	xHO2 + RO2C + xCCHO + yROOH	k<304>= 1.340E-12 * (T/300)**(2.00) * exp(-499.0/T)
{BL02}	ALK2 + OH	--->	0.965*xHO2 +0.965*RO2C +0.035*RO2XC +0.035*zRNO3 +0.261*xRCHO +0.704*xACETONE + yROOH	k<305>= 1.490E-12 * (T/300)**(2.00) * exp(-87.0/T)
{BL03}	ALK3 + OH	--->	0.695*xHO2 +0.236*xTBUO +1.253*RO2C +0.07*RO2XC +0.07*zRNO3 +0.026*xHCHO +0.445*xCCHO +0.122*xRCHO +0.024*xACETONE +0.332*xMEK +0.983*yROOH +0.017*yR6OOH	k<306>= 1.510E-12 * exp(126.0/T)
{BL04}	ALK4 + OH	--->	0.830*xHO2 +0.010*xMEO2 +0.011*xMECO3 +1.763*RO2C +0.149*RO2XC +0.149*zRNO3 +0.002*xCO +0.029*xHCHO +0.438*xCCHO +0.236*xRCHO +0.426*xACETONE +0.106*xMEK +0.146*xPROD2 + yR6OOH	k<307>= 3.750E-12 * exp(44.0/T)
{BL05}	ALK5 + OH	--->	0.647*xHO2 +1.605*RO2C +0.353*RO2XC +0.353*zRNO3 +0.04*xHCHO +0.106*xCCHO +0.209*xRCHO +0.071*xACETONE +0.086*xMEK +0.407*xPROD2 + yR6OOH + ALK5RXN	k<308>= 2.700E-12 * exp(374.0/T)

{BL06}	OLE1	+ OH	--->	0.871*xHO2 +0.001*xMEO2 +1.202*RO2C +0.128*RO2XC +0.128*zRNO3 +0.582*xHCHO +0.01*xCCHO +0.007*xHOCCHO +0.666*xRCHO +0.007*xACETONE +0.036*xACROLEIN +0.001*xMACR +0.012*xMVK +0.009*xIPRD +0.168*xPROD2 +0.169*yROOH +0.831*yR6OOH	k<309>= 6.720E-12 * exp(501.0/T)
{BL07}	OLE1	+ O3	--->	0.095*HO2 +0.057*xHO2 +0.128*OH +0.09*RO2C +0.005*RO2XC +0.005*zRNO3 +0.303*CO +0.088*CO2 +0.5*HCHO +0.011*xCCHO +0.5*RCHO +0.044*xRCHO +0.003*xACETONE +0.009*MEK +0.185*HCOOH +0.159*RCOOH +0.268*PRD2 +0.011*yROOH	k<310>= 3.190E-15 * exp(-1701.0/T)
{BL08}	OLE1	+ NO3	--->	0.772*xHO2 +1.463*RO2C +0.228*RO2XC +0.228*zRNO3 +0.013*xCCHO +0.003*xRCHO +0.034*xACETONE +0.774*xRNO3 +0.169*yROOH +0.831*yR6OOH	k<311>= 5.370E-13 * exp(-1047.0/T)
{BL09}	OLE1	+ O3P	--->	0.450*RCHO +0.390*MEK +0.160*PRD2	k<312>= 1.610E-11 * exp(-326.0/T)
{BL10}	OLE2	+ OH	--->	0.912*xHO2 +0.953*RO2C +0.088*RO2XC +0.088*zRNO3 +0.179*xHCHO +0.835*xCCHO +0.51*xRCHO +0.144*xACETONE +0.08*xMEK +0.002*xMVK +0.012*xIPRD +0.023*xPROD2 +0.319*yROOH +0.681*yR6OOH	k<313>= 1.260E-11 * exp(488.0/T)
{BL11}	OLE2	+ O3	--->	0.094*HO2 +0.041*xHO2 +0.443*OH +0.307*MEO2 +0.156*xMECO3 +0.008*xRCO3 +0.212*RO2C +0.003*RO2XC +0.003*zRNO3 +0.299*CO +0.161*CO2 +0.131*HCHO +0.114*xHCHO +0.453*CCHO +0.071*xCCHO +0.333*RCHO +0.019*xRCHO +0.051*ACETONE	k<314>= 8.590E-15 * exp(-1255.0/T)
{BL12}	OLE2	+ NO3	--->	0.400*xHO2 +0.426*xNO2 +0.035*xMEO2 +1.193*RO2C +0.14*RO2XC +0.14*zRNO3 +0.072*xHCHO +0.579*xCCHO +0.163*xRCHO +0.116*xACETONE +0.002*xMEK +0.32*xRNO3 +0.319*yROOH +0.681*yR6OOH	k<315>= 2.310E-13 * exp(382.0/T)
{BL13}	OLE2	+ O3P	--->	0.079*RCHO +0.751*MEK +0.170*PRD2	k<316>= 1.430E-11 * exp(111.0/T)
{BL14}	ARO1	+ OH	--->	0.123*HO2 +0.566*xHO2 +0.202*OH +0.566*RO2C +0.11*RO2XC +0.11*zRNO3 +0.158*xGLY +0.1*xMGLY +0.123*CRES +0.072*xAFG1 +0.185*xAFG2 +0.202*AFG3 +0.309*xPROD2 +0.369*yR6OOH + TOLRO2	k<317>= 7.840E-12
{BL15}	ARO2	+ OH	--->	0.077*HO2 +0.617*xHO2 +0.178*OH +0.617*RO2C +0.128*RO2XC +0.128*zRNO3 +0.088*xGLY +0.312*xMGLY +0.134*xBACL +0.077*CRES +0.026*xBALD +0.221*xAFG1 +0.247*xAFG2 +0.178*AFG3 +0.068*xAFG3 +0.057*xPROD2 +0.101*yR6OOH + XYLRO2	k<318>= 3.090E-11
{BL16}	TERP	+ OH	--->	0.734*xHO2 +0.064*xRCO3 +1.211*RO2C +0.201*RO2XC +0.201*zRNO3 +0.001*xCO +0.411*xHCHO +0.385*xRCHO +0.037*xACETONE +0.007*xMEK +0.003*xMGLY +0.009*xBACL +0.003*xMVK +0.002*xIPRD +0.409*xPROD2 + yR6OOH + TRPRXN	k<319>= 2.270E-11 * exp(435.0/T)
{BL17}	TERP	+ O3	--->	0.078*HO2 +0.046*xHO2 +0.499*OH +0.202*xMECO3 +0.059*xRCO3 +0.49*RO2C +0.121*RO2XC +0.121*zRNO3 +0.249*CO +0.063*CO2 +0.127*HCHO +0.033*xHCHO +0.208*xRCHO +0.057*xACETONE +0.002*MEK +0.172*HCOOH +0.068*RCOOH +0.003*xMGLY	k<320>= 8.280E-16 * exp(-785.0/T)
{BL18}	TERP	+ NO3	--->	0.227*xHO2 +0.287*xNO2 +0.026*xRCO3 +1.786*RO2C +0.46*RO2XC +0.46*zRNO3 +0.012*xCO +0.023*xHCHO +0.002*xHOCCHO +0.403*xRCHO +0.239*xACETONE +0.005*xMACR +0.001*xMVK +0.004*xIPRD +0.228*xRNO3 + yR6OOH + TRPRXN	k<321>= 1.330E-12 * exp(490.0/T)
{BL19}	TERP	+ O3P	--->	0.237*RCHO +0.763*PRD2 + TRPRXN	k<322>= 4.020E-11

{BT19}	SESQ	+ OH	--->	0.734*xHO2 +0.064*xRCO3 +1.211*RO2C +0.201*RO2XC +0.201*zRNO3 +0.001*xCO +0.411*xHCHO +0.385*xRCHO +0.037*xACETONE +0.007*xMEK +0.003*xMGLY +0.009*xBACL +0.003*xMVK +0.002*xIPRD +0.409*xPROD2 + yR6OOH + SESQRXN	k<323> = 1.000E+00 * k(BL16)
{BT20}	SESQ	+ O3	--->	0.078*HO2 +0.046*xHO2 +0.499*OH +0.202*xMECO3 +0.059*xRCO3 +0.49*RO2C +0.121*RO2XC +0.121*zRNO3 +0.249*CO +0.063*CO2 +0.127*HCHO +0.033*xHCHO +0.208*xRCHO +0.057*xACETONE +0.002*MEK +0.172*HCOOH +0.068*RCOOH +0.003*xMGLY	k<324> = 1.000E+00 * k(BL17)
{BT21}	SESQ	+ NO3	--->	0.227*xHO2 +0.287*xNO2 +0.026*xRCO3 +1.786*RO2C +0.46*RO2XC +0.46*zRNO3 +0.012*xCO +0.023*xHCHO +0.002*xCCHO +0.403*xRCHO +0.239*xACETONE +0.005*xMACR +0.001*xMVK +0.004*xIPRD +0.228*xRNO3 + yR6OOH + SESQRXN	k<325> = 1.000E+00 * k(BL18)
{BT22}	SESQ	+ O3P	--->	0.237*RCHO +0.763*PRD2 + SESQRXN	k<326> = 1.000E+00 * k(BL19)

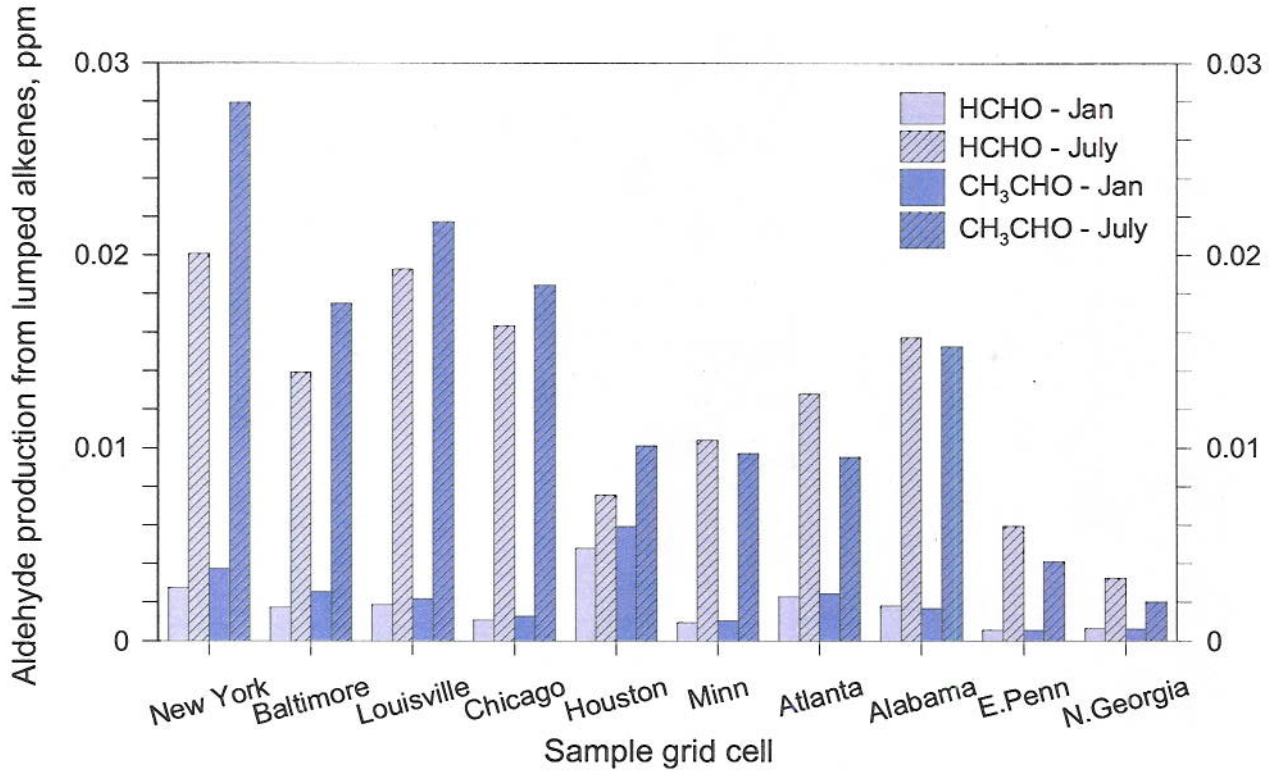

Figure S-1: Comparison of absolute amount of HCHO and CH_3CHO formed over 72 hours periods from lumped alkenes in January and July. Totals are shown for 6 grids. Overall HCHO formation is generally 20-50 times larger in July than January, and overall CH_3CHO formation is 10-20 times larger in July.

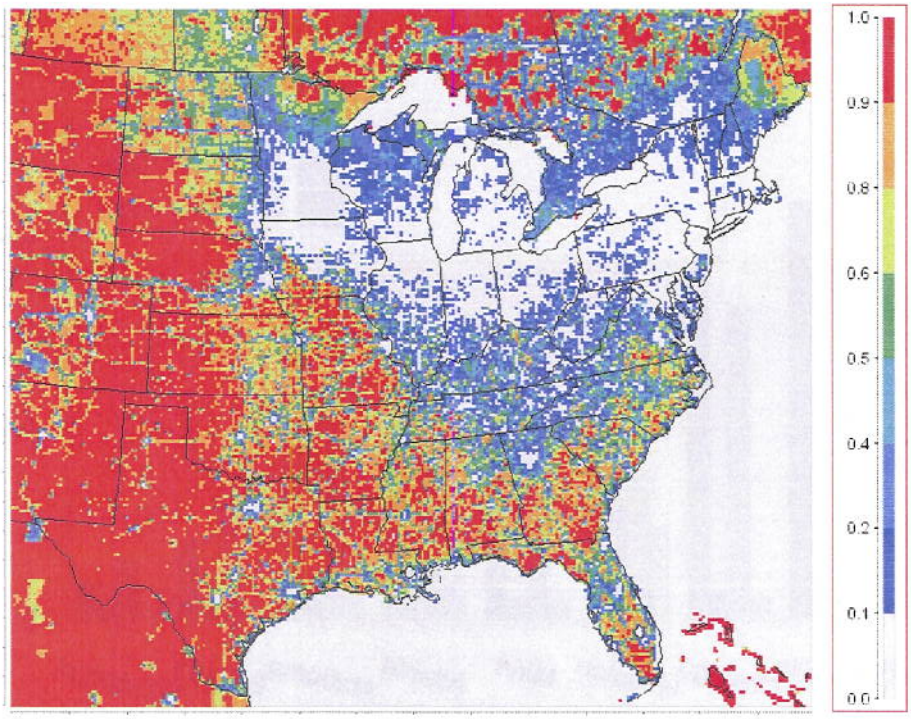

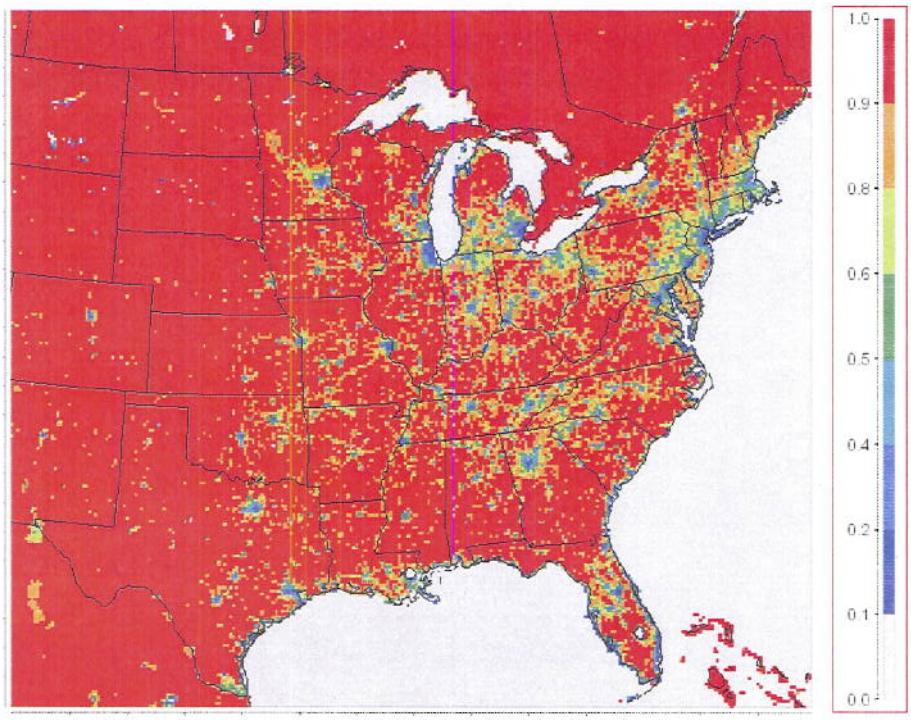

Figure S-2: Fraction of total lumped alkene emissions due to biogenic sources in January (top) and July (bottom).

References

Hutzell, W.T., Luecken, D.J., Appel, K.W., Carter, W.P.L., 2011. Interpreting predictions from the SAPRC07 mechanism based on regional and continental simulations. Atmospheric Environment, in press.